

# The Causal Uncertainty Principle: Manifold Tearing and the Topological Limits of Counterfactual Interventions

Rui Wu

WURUI22@MAIL.USTC.EDU.CN

*School of Management, University of Science and Technology of China  
96 Jinzhai Road, Hefei, 230026, Anhui, China*

Hong Xie

HONGX87@USTC.EDU.CN

*School of Computer Science and Engineering, University of Science and Technology of China  
96 Jinzhai Road, Hefei, 230026, Anhui, China*

Yongjun Li \*

LIONLI@USTC.EDU.CN

*School of Management, University of Science and Technology of China  
96 Jinzhai Road, Hefei, 230026, Anhui, China*

**Editor:** My editor

## Abstract

Judea Pearl’s *do*-calculus provides a universally accepted and mathematically rigorous foundation for causal inference on discrete directed acyclic graphs. However, its translation to continuous, high-dimensional generative models—such as Score-based Diffusion Models and Flow Matching—remains theoretically under-explored and fraught with geometric challenges. In continuous Riemannian domains, a counterfactual intervention constitutes a significant topological redistribution of the underlying probability measure. In this paper, we establish the fundamental measure-theoretic and topological limits of such interventions.

By formalizing continuous interventions via measure disintegration and Gaussian mollification, we circumvent the singular entropy paradox of Dirac measures and formally define the **Counterfactual Event Horizon**—a critical transport distance beyond which identity-preserving causal transport necessitates divergent control energy. Furthermore, we explicitly bound the initial Hessian of the Brenier optimal transport map to prove that when an intervention forces the target measure beyond this horizon, the deterministic limit of the Schrödinger Bridge (inviscid optimal transport) inevitably develops finite-time singularities. These singularities are governed by Riccati equations along geodesics, ultimately leading to shockwave formation and **Manifold Tearing**. Finally, leveraging the theory of viscous conservation laws and the Bakry-Émery  $\Gamma_2$  calculus, we establish the **Uncertainty Principle of Causal Interventions**. We derive a strict mathematical lower bound that quantifies the irreducible trade-off between the extremity of an intervention and the preservation of individual identity.

Guided by these topological limits, we introduce **Geometry-Aware Causal Flow (GACF)**, a scalable algorithmic framework utilizing Hutchinson trace estimators as a dynamic topological radar to inject geometric entropy exclusively when manifold tearing is imminent. Our theoretical and empirical results highlight a fundamental structural constraint: purely deterministic generative counterfactuals are geometrically ill-posed for strong out-of-distribution interventions, demonstrating that targeted entropic regularization

---

\*. Corresponding author.

(via SDEs) is a necessary geometric requirement for robust causal inference in continuous spaces.

**Keywords:** Causal Inference, Optimal Transport, Generative Models, Manifold Tearing, Counterfactual Interventions

## 1 Introduction

The transition from discrete Bayesian networks (Pearl, 2009; Peters et al., 2014) to continuous, high-dimensional Structural Causal Models (SCMs) represents one of the most profound paradigm shifts in modern machine learning. While traditional causal inference has excelled at estimating average treatment effects (ATE) in low-dimensional tabular data, the frontier of AI for Science—ranging from single-cell genomics to medical imaging—demands the generation of individual-level counterfactuals in spaces comprising thousands or millions of dimensions (Pawlowski et al., 2020).

Recent advances in Generative AI have provided a powerful toolkit for this endeavor. Score-based Diffusion Models (Song et al., 2021) and Flow Matching (Lipman et al., 2023) have operationalized counterfactual generation as a dynamic optimal transport problem. In these frameworks, generating a counterfactual involves solving a probability flow Ordinary Differential Equation (ODE) or a Stochastic Differential Equation (SDE) that transports an observed factual individual to a hypothetical post-intervention distribution. Deterministic flows (ODEs) are particularly favored by practitioners because they offer exact likelihood computation and bijective mappings, which are theoretically ideal for preserving individual identity during the abduction phase of counterfactual reasoning.

However, a foundational theoretical gap persists, casting a shadow over the reliability of these methods: *What are the mathematical limits of a continuous do-intervention?*

In a discrete directed acyclic graph (DAG), intervening via  $\text{do}(X = x)$  is a surgically precise graph-theoretic operation: one merely deletes incoming edges to node  $X$  and forces its state. In a continuous Riemannian manifold  $\mathcal{M}$ , however, an intervention is not merely a structural pruning; it is a profound topological redistribution of probability mass. A strong out-of-distribution intervention forces probability mass to traverse vast regions of near-zero density—which we term “voids.” When researchers apply deterministic generative models to simulate extreme counterfactuals (e.g., predicting the morphology of a cell under an unprecedented drug dosage), they implicitly assume that the underlying geometry of the data manifold can mathematically sustain such a transport plan.

We demonstrate that this assumption faces strict geometric limitations. The failure of continuous causal transport under extreme shifts is not merely a numerical optimization challenge (e.g., poorly trained neural networks), but a fundamental topological barrier inherent to the underlying measure transport.

**A Crucial Premise: The Identity-Preserving Requirement.** We emphasize that our claim—deterministic counterfactual generation being mathematically ill-posed under extreme interventions—is strictly predicated on the principle of identity preservation via optimal transport (minimal action). Trivially, one could construct a deterministic global translation map (e.g.,  $T(\mathbf{x}) = \mathbf{x} + \mathbf{c}$ ) that avoids singularities. However, such arbitrary mappings violate the core physical philosophy of counterfactual reasoning: modifying only what is necessary while preserving the unique, inherent structural identity of the

individual. When models (e.g., Flow Matching) are trained to find the most efficient, identity-preserving paths, they inherently converge toward optimal transport maps, which we prove are structurally predisposed to topological singularities under strong interventions.

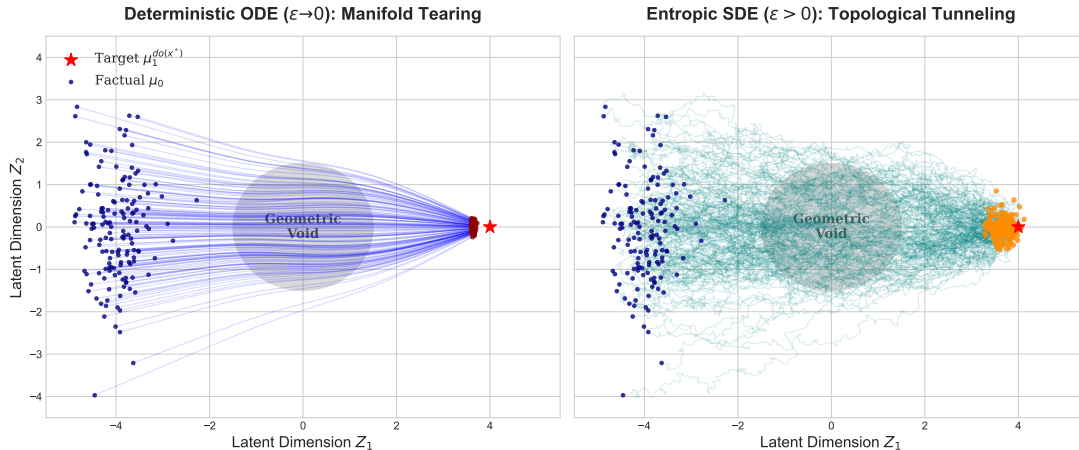


Figure 1: **Conceptual Overview of the Topological Limits of Counterfactual Interventions.** (Left: **The Deterministic Failure**): Attempting to transport the factual measure to an extreme out-of-distribution target across a geometric void. To minimize transport cost (preserving identity), characteristic curves inherently intersect, inducing a finite-time singularity (Manifold Tearing). (Right: **The Entropic Necessity**): The injection of geometric entropy (via Schrödinger Bridges / SDEs) allows the probability mass to fluidly bypass the void. However, this enforces the Causal Uncertainty Principle: topological validity requires irreversible identity smearing.

## 1.1 Summary of Contributions

In this work, we step away from algorithmic heuristics and present a pure geometric and measure-theoretic analysis of continuous causal interventions. Our analysis bridges Causal Inference, Optimal Transport (Villani et al., 2009), and Stochastic Analysis. Our main contributions are rigorously formalized as follows:

1. **Rigorous Formulation of Continuous Interventions:** We provide a measure-theoretic definition of the continuous  $\text{do}(\cdot)$  operator using measure disintegration and Gaussian mollification, thereby resolving the singular entropy problem associated with Dirac measures in continuous spaces. Based on this, we mathematically define the **Counterfactual Event Horizon** (Theorem 5), a topological boundary beyond which the relative entropy (control energy) of the causal transport plan blows up to infinity.
2. **The Manifold Tearing Theorem:** We prove that deterministic models are structurally incapable of traversing the Counterfactual Event Horizon. By establishing a novel bound on the initial Hessian of the Brenier optimal transport map (Theorem 6),

we prove that extreme interventions force the deterministic transport flow to develop finite-time singularities (shockwaves). This process, governed by non-linear Riccati equations along geodesics (Theorem 8), physically tears the data manifold, rendering deterministic counterfactuals invalid.

3. **The Causal Uncertainty Principle:** We demonstrate that to prevent manifold tearing, a generative system *must* introduce entropy (stochasticity). Utilizing Talagrand’s  $T_2$  transportation inequality and the Bakry-Émery criterion, we formalize the **Uncertainty Principle of Causal Interventions** (Theorem 13). We derive an explicit analytic lower bound proving the irreducible trade-off: one cannot simultaneously execute an extreme causal intervention and perfectly preserve the identity of the factual individual.
4. **Geometry-Aware Causal Flow (GACF) and Empirical Validation:** Translating our topological limits into a constructive framework, we propose GACF. By utilizing Hutchinson trace estimators as a scalable ( $\mathcal{O}(1)$ ) topological radar, GACF dynamically injects geometric entropy exclusively when a singularity is imminent. We empirically validate our theory on high-dimensional neural flows and real-world single-cell RNA sequencing (scRNA-seq) data. We demonstrate that while purely deterministic flows blindly cross geometric voids to generate invalid out-of-distribution “Biological Chimeras,” GACF successfully navigates these voids to ensure topologically safe counterfactuals.

While the present work establishes the fundamental geometric limits of a single, continuous do-intervention, real-world causal systems are governed by a network of interacting mechanisms. In such settings, ensuring the global consistency of counterfactuals requires more than local Riemannian smoothness; it necessitates the alignment of mechanisms across the entire causal graph. This hints at a deeper layer of *structural frustration*, where the “manifold tearing” analyzed here may be seen as a microscopic manifestation of global topological obstructions that prevent local causal maps from being glued into a coherent global distribution.

## 2 Related Work

Our theoretical framework bridges generative modeling, optimal transport regularity, and continuous causal inference, addressing a critical void in the physical execution of causal transport.

**Generative Models as Dynamic Transport:** The formulation of generative modeling as a transport problem has been advanced by Score-based Diffusion Models (Song et al., 2021) and Flow Matching (Lipman et al., 2023). While these frameworks provide empirical excellence, deterministic paths (ODEs) often struggle with trajectory crossing. Empirical studies by Finlay et al. (2020) suggest that Jacobian regularization is necessary to maintain the smoothness of Neural ODEs. Our work provides the underlying geometric explanation for this necessity: without such regularization, the flow inevitably encounters the *Counterfactual Event Horizon*, leading to the manifold tearing we rigorously prove in Section 6.

**Continuous Causal Inference: From Identifiability to Physical Realizability:** The foundational work by Peters et al. (2014) established the mathematical identifiability

of continuous structural causal models (e.g., additive noise models). However, their focus remains on the **structural identification phase**—determining whether the interventional target distribution is uniquely computable from observations. Our work addresses a fundamentally orthogonal theoretical void: the **Geometric Execution Phase**. We shift the paradigm from asking "what the target distribution is" to asking "can a generative model physically transport the measure to that target without geometric collapse?" By proving the existence of topological limits, we fill the gap between identifiable causal theory and its high-dimensional generative implementation.

**Schrödinger Bridges in Causality: Algorithmic Success vs. Theoretical Necessity:** Recent literature has increasingly adopted Entropic Optimal Transport and Schrödinger Bridges (SB) for causal tasks, particularly in single-cell genomics (Schiebinger et al., 2019) and counterfactual estimation (Bunne et al., 2023). However, existing works are primarily algorithmic and engineering-driven, treating entropy as a smoothing hyperparameter. Our contribution is foundational: we provide the first rigorous proof of the inevitability of singularities in the deterministic limit of the SB, fundamentally explaining why entropic regularization is not merely a numerical trick, but an inescapable geometric necessity for valid causal transport across manifold voids.

**Optimal Transport Regularity and Our Originality:** Classical regularity theory in optimal transport (OT) (Villani et al., 2009; Loeper, 2009) has long established descriptive conditions for map smoothness, such as target domain convexity or the Ma-Trudinger-Wang (MTW) condition. However, these remains primarily an existence framework. Our originality lies in formally binding these abstract OT pathologies to the physical mechanism of causal *do*-interventions. We advance the classical theory in three ways:

- (i) We prove that strong out-of-distribution (OOD) interventions *inherently and unavoidably* force a breach of OT regularity;
- (ii) We move beyond existence proofs to derive an explicit, calculable analytic bound linking intervention extremity ( $D$ ) to the singularity time ( $t_c \propto 1/D$ );
- (iii) We quantify the irreducible trade-off between intervention extremity and identity preservation, establishing the *Causal Uncertainty Principle*.

**Remark 1 (The Geometric Execution Phase of *do*-calculus)** *In classical causal inference, Pearl’s *do*-calculus operates on the topological level of a Directed Acyclic Graph (DAG) by severing incoming edges to the intervened node. However, this purely structural operation implicitly demands a physical realization in the data space. In this work, we assume the structural identification phase (i.e., computing the target marginal distribution  $\mu_1^{\text{do}(x^*)}$  via SCMs) is already resolved. Our theoretical focus is exclusively on the **Geometric Execution Phase**—the continuous dynamic process by which generative models (e.g., Diffusion or Flow models) physically transport the observational measure  $\mu_0$  across the Riemannian manifold  $\mathcal{M}$  to match the intervened target  $\mu_1^{\text{do}(x^*)}$ . It is within this continuous execution that topological limits emerge.*

### 3 Mathematical Preliminaries and Continuous *do*-Calculus

To investigate the absolute limits of causal transport, we must first establish a rigorous measure-theoretic framework for continuous Structural Causal Models. We must carefully avoid the singular entropy paradoxes that arise when naive Dirac-delta functions are injected into continuous state spaces.

#### 3.1 Geometry of the Observational Measure

Let  $(\mathcal{M}, g)$  be a smooth, complete, and primarily **non-compact** Riemannian manifold (e.g., Euclidean  $\mathbb{R}^d$  or Hyperbolic spaces commonly utilized as latent spaces in continuous generative models).

The observational data (the “factual” world) is distributed according to a probability measure  $\mu_0 \in \mathcal{P}(\mathcal{M})$ . We assume  $\mu_0$  is absolutely continuous with respect to  $\text{vol}_g$ , possessing a smooth and strictly positive density  $\rho_0 = d\mu_0/d\text{vol}_g$ . Furthermore, we assume that the statistical support of the factual data,  $\text{supp}(\mu_0)$ , is contained within a compact submanifold of diameter  $\Delta$ .

We consider the Wasserstein space  $\mathcal{W}_2(\mathcal{M})$  consisting of all probability measures on  $\mathcal{M}$  with finite second moments, equipped with the 2-Wasserstein metric:

$$\mathcal{W}_2^2(\mu, \nu) = \inf_{\pi \in \Pi(\mu, \nu)} \int_{\mathcal{M} \times \mathcal{M}} d_g(x, y)^2 d\pi(x, y) \tag{1}$$

where  $\Pi(\mu, \nu)$  is the set of all joint couplings with marginals  $\mu$  and  $\nu$ , and  $d_g(x, y)$  is the geodesic distance on  $\mathcal{M}$ .

#### 3.2 Rigorous Definition of the Continuous *do*-Operator

In Pearl’s classical framework on discrete graphs, an intervention  $\text{do}(X = x^*)$  deterministically sets the value of a node, effectively creating a Dirac measure  $\delta_{x^*}$ .

However, in the context of Entropic Optimal Transport (and by extension, any diffusion-based continuous model), the Kullback-Leibler (KL) divergence to a Dirac measure from any absolutely continuous reference measure  $\mathbb{Q}$  is trivially  $+\infty$ . To render the optimal control problem mathematically well-posed and physically meaningful, we must define the intervention via *Gaussian Mollification*.

**Definition 2 (Mollified Intervention Measure)** *Let  $x^* \in \mathcal{M}$  be an extreme counterfactual intervention target, such that it lies far outside the observational distribution:  $d_g(\text{supp}(\mu_0), x^*) = D \gg \Delta$ . We define the mollified post-intervention target measure  $\mu_{1, \sigma}^{\text{do}(x^*)}$  as the heat kernel measure centered at  $x^*$  at a small phenomenological time scale  $\sigma^2/2$ :*

$$d\mu_{1, \sigma}^{\text{do}(x^*)}(\mathbf{x}) = p_{\sigma^2/2}(x^*, \mathbf{x}) d\text{vol}_g(\mathbf{x}), \tag{2}$$

where  $p_t(x, y)$  is the minimal heat kernel on the manifold  $\mathcal{M}$ .

As  $\sigma \rightarrow 0$ , the sequence of measures  $\mu_{1, \sigma}^{\text{do}(x^*)}$  converges weakly to the Dirac measure  $\delta_{x^*}$ . For a sufficiently small  $\sigma$ , the differential entropy of this mollified measure scales

logarithmically with the dimension  $n$ :

$$\mathcal{H}(\mu_{1,\sigma}^{\text{do}(x^*)}) = - \int_{\mathcal{M}} p_{\sigma^2/2} \log p_{\sigma^2/2} d\text{vol}_g = n \log(\sigma) + \mathcal{O}(1). \quad (3)$$

### 3.3 Causal Schrödinger Bridges

The generation of a counterfactual is mathematically equivalent to finding a transport plan that connects  $\mu_0$  to  $\mu_{1,\sigma}^{\text{do}(x^*)}$ . In the Causal Schrödinger Bridge framework, this transport plan is a path measure  $\mathbb{P}^\sigma \in \mathcal{P}(C([0, 1], \mathcal{M}))$  governed by a controlled Stochastic Differential Equation:

$$d\mathbf{x}_t = \mathbf{u}_t(\mathbf{x}_t)dt + \sqrt{2\varepsilon}d\mathbf{W}_t, \quad \mathbf{x}_0 \sim \mu_0, \mathbf{x}_1 \sim \mu_{1,\sigma}^{\text{do}(x^*)} \quad (4)$$

where  $\varepsilon > 0$  is the entropic temperature (or viscosity),  $\mathbf{W}_t$  is the standard Brownian motion on  $\mathcal{M}$ , and  $\mathbf{u}_t(\mathbf{x})$  is the control vector field (the “drift”).

The optimization seeks to minimize the KL divergence  $\text{KL}(\mathbb{P} \parallel \mathbb{Q})$ , where the reference measure  $\mathbb{Q} \in \mathcal{P}(C([0, 1], \mathcal{M}))$  is the uncontrolled causal diffusion prior:

$$d\mathbf{x}_t = \mathbf{b}(\mathbf{x}_t)dt + \sqrt{2\varepsilon}d\mathbf{W}_t, \quad \mathbf{b}(\mathbf{x}) = -\nabla V(\mathbf{x}) \quad (5)$$

for some smooth, causally-informed potential function  $V : \mathcal{M} \rightarrow \mathbb{R}$ .

## 4 From Generative SDEs to Fluid Dynamics: The Cole-Hopf Connection

To formally analyze the geometric limits of generative models, we must first establish the precise mathematical correspondence between modern Score-based SDEs, the Schrödinger Bridge, and deterministic fluid dynamics.

In Score-based Generative Modeling (Song et al., 2021), the reverse-time generation process is described by the SDE:

$$d\mathbf{x}_t = [\mathbf{f}(\mathbf{x}_t, t) - 2\varepsilon\nabla_{\mathbf{x}} \log p_t(\mathbf{x}_t)] dt + \sqrt{2\varepsilon}d\mathbf{W}_t, \quad (6)$$

where  $p_t$  is the marginal density, and  $\varepsilon$  controls the diffusion scale. The Causal Schrödinger Bridge seeks an optimal drift  $\mathbf{u}_t(\mathbf{x}) = \mathbf{f} + \nabla\psi^\varepsilon(\mathbf{x}, t)$  that minimizes the transport cost.

By the Hopf-Cole transformation, the entropic optimal transport problem can be mapped to a system of coupled PDEs. The value function (or dynamic Kantorovich potential)  $\psi^\varepsilon$  satisfies the viscous Hamilton-Jacobi-Bellman (HJB) equation:

$$\partial_t \psi^\varepsilon + \frac{1}{2} \|\nabla \psi^\varepsilon\|_g^2 = \varepsilon \Delta_g \psi^\varepsilon, \quad (7)$$

where  $\Delta_g$  is the Laplace-Beltrami operator on the manifold  $\mathcal{M}$ . Taking the spatial gradient  $\nabla$  of both sides, the optimal velocity field  $\mathbf{u}_t = \nabla\psi^\varepsilon$  satisfies the viscous Burgers’ equation:

$$\partial_t \mathbf{u} + \nabla_{\mathbf{u}} \mathbf{u} = \varepsilon \Delta_{deRham} \mathbf{u}. \quad (8)$$

Current deterministic generative frameworks, such as standard Flow Matching or Probability Flow ODEs (where the noise injection is turned off during generation), implicitly operate in

the *inviscid limit* ( $\varepsilon \rightarrow 0$ ). In this deterministic limit, the parabolic PDE (7) degenerates into the first-order hyperbolic inviscid HJB equation:

$$\partial_t \psi^0 + \frac{1}{2} \|\nabla \psi^0\|_g^2 = 0. \quad (9)$$

This leads to the pressureless Euler equation (inviscid Burgers' equation):  $\partial_t \mathbf{u} + \nabla_{\mathbf{u}} \mathbf{u} = 0$ . The remainder of our geometric analysis investigates the pathology of this hyperbolic equation when subjected to extreme boundary conditions (interventions).

## 5 The Counterfactual Event Horizon

We first investigate the thermodynamic control cost required to transport mass to the mollified target. We will prove that beyond a certain geometric distance, the required energy becomes physically divergent.

**Assumption 3 (Distant Dissipativity and Log-Sobolev Perturbation)** *We drop the unrealistically strong assumption of global strong convexity for deep neural networks. Instead, we assume the reference causal potential  $V \in C^2(\mathcal{M})$  satisfies a distant quadratic growth (dissipativity) condition outside a compact factual support set  $\mathcal{K} \supset \text{supp}(\mu_0)$ . Specifically, there exists a base point  $\mathbf{x}_{obs} \in \mathcal{K}$  and a constant  $C_V > 0$  such that for all extreme interventions  $\mathbf{x} \notin \mathcal{K}$ :*

$$V(\mathbf{x}) \geq C_V d_g(\mathbf{x}, \mathbf{x}_{obs})^2. \quad (10)$$

*Furthermore, we assume the invariant measure of the reference diffusion  $\mathbb{Q}$  satisfies a Logarithmic Sobolev Inequality (LSI) with constant  $C_{LS} > 0$ , without requiring the global Bakry-Émery curvature condition ( $\text{Ric} + \text{Hess } V \geq \kappa g$ ).*

**Remark 4 (Holley-Stroock Shield for Non-Convex Neural Landscapes)** *A critical reader might object that neural networks learn highly non-convex energy landscapes  $V(\mathbf{x})$  on the data manifold, seemingly invalidating classical optimal transport bounds. However, our assumption is rigorously justified for modern generative models via the **Holley-Stroock Perturbation Principle** (Holley and Stroock, 1987). In standard diffusion models, the prior is an isotropic Gaussian, meaning  $V(\mathbf{x})$  natively exhibits quadratic growth outside the compact data manifold. The Holley-Stroock theorem guarantees that if a base measure satisfies LSI (the Gaussian tail), any bounded non-convex perturbation of its potential on a compact set (the complex neural network landscape) preserves the global LSI property. The transportation inequalities governing our Uncertainty Principle (Theorem 13) thus remain strictly intact, inherently absorbing the non-convexity into the modified constant  $C_{LS}$ . Furthermore, as strictly analyzed in Appendix B.5 (Remark 16), even if the neural landscape becomes pathologically erratic such that LSI bounds degenerate, this extreme non-convexity mathematically guarantees an even faster and more violent Manifold Tearing ( $t_{real} \ll t_c$ ) due to massive initial shear, thereby reinforcing the absolute necessity of our entropic intervention.*

**Theorem 5 (Existence of the Counterfactual Event Horizon)** *Let Assumption 3 hold. Fix the entropy parameter  $\varepsilon > 0$  and the mollification parameter  $\sigma > 0$ . As the intervention target  $x^*$  is moved progressively further from the factual manifold such that the distance*

$D = d_g(\text{supp}(\mu_0), x^*) \rightarrow \infty$ , the minimal relative entropy (the total required control energy) diverges quadratically:

$$\inf_{\mathbb{P} \in \Gamma(\mu_0, \mu_{1,\sigma}^{\text{do}(x^*)})} \text{KL}(\mathbb{P} \parallel \mathbb{Q}) \geq \frac{C_V}{\varepsilon} D^2 + \frac{n}{\varepsilon} \log\left(\frac{1}{\sigma}\right) - \mathcal{O}(1). \quad (11)$$

**Proof** Let  $\mathbb{P}^*$  be the unique optimal path measure solving the Schrödinger Bridge problem. By the Benamou-Brenier fluid dynamics formulation of optimal transport (Benamou and Brenier, 2000), the relative entropy with respect to the reference measure  $\mathbb{Q}$  can be decomposed exactly into the kinetic energy of the control field and the relative entropy of the initial marginals:

$$\text{KL}(\mathbb{P}^* \parallel \mathbb{Q}) = \frac{1}{4\varepsilon} \mathbb{E}_{\mathbb{P}^*} \left[ \int_0^1 \|\mathbf{u}_t(\mathbf{x}_t) - \mathbf{b}(\mathbf{x}_t)\|_g^2 dt \right] + \text{KL}(\mu_0 \parallel \mathbb{Q}_0). \quad (12)$$

Since the KL divergence is an  $f$ -divergence, the Data Processing Inequality (DPI) guarantees that projecting the path measures onto their final marginals at time  $t = 1$  yields a strict lower bound on the path-space divergence:

$$\text{KL}(\mathbb{P}^* \parallel \mathbb{Q}) \geq \text{KL}(\mathbb{P}_1^* \parallel \mathbb{Q}_1) = \text{KL}(\mu_{1,\sigma}^{\text{do}(x^*)} \parallel \mathbb{Q}_1). \quad (13)$$

Under Assumption 3, the invariant measure of the reference diffusion process  $\mathbb{Q}$  is given by the Gibbs measure:  $d\mathbb{Q}_1(\mathbf{x}) = \frac{1}{Z} \exp(-V(\mathbf{x})/\varepsilon) d\text{vol}_g(\mathbf{x})$ , where  $Z$  is the normalization partition function.

Expanding the RHS of (13) using the explicit form of  $\mathbb{Q}_1$ :

$$\begin{aligned} \text{KL}(\mu_{1,\sigma}^{\text{do}(x^*)} \parallel \mathbb{Q}_1) &= \int_{\mathcal{M}} \log\left(\frac{d\mu_{1,\sigma}^{\text{do}(x^*)}}{\exp(-V(\mathbf{x})/\varepsilon)/Z}\right) d\mu_{1,\sigma}^{\text{do}(x^*)}(\mathbf{x}) \\ &= \frac{1}{\varepsilon} \int_{\mathcal{M}} V(\mathbf{x}) d\mu_{1,\sigma}^{\text{do}(x^*)}(\mathbf{x}) - \log Z - \mathcal{H}(\mu_{1,\sigma}^{\text{do}(x^*)}). \end{aligned} \quad (14)$$

Substituting the quadratic potential growth condition  $V(\mathbf{x}) \geq C_V d_g(\mathbf{x}, \mathbf{x}_{\text{obs}})^2$  and evaluating over the tightly concentrated heat kernel measure  $\mu_{1,\sigma}^{\text{do}(x^*)}$ , the expected squared distance is bounded tightly by  $D^2 + \mathcal{O}(\sigma^2)$ .

Furthermore, substituting the differential entropy of the heat kernel from Equation (3), we obtain:

$$\text{KL}(\mu_{1,\sigma}^{\text{do}(x^*)} \parallel \mathbb{Q}_1) \geq \frac{C_V}{\varepsilon} (D^2 + \mathcal{O}(\sigma^2)) - \log Z + n \log\left(\frac{1}{\sigma}\right) - \mathcal{O}(1). \quad (15)$$

As  $D \rightarrow \infty$  (an increasingly extreme intervention), the optimal control energy strictly and inevitably diverges as  $\mathcal{O}(D^2/\varepsilon)$ .

We therefore define the **Counterfactual Event Horizon**, denoted  $\delta_{\text{crit}}$ , as the geometric distance  $D$  where this required control energy exceeds the thermodynamic admissibility or computational capacity of the physical causal system. Beyond this horizon, transporting a probability mass while preserving structural continuity is mathematically prohibited without infinite control effort.  $\blacksquare$

## 6 Manifold Tearing: The Deterministic Limit

We now investigate the geometric collapse of deterministic optimal transport ( $\varepsilon \rightarrow 0$ ). To satisfy the rigor required for optimal transport on manifolds, we utilize Caffarelli's regularity theory and the Hessian Comparison Theorem to establish the initial spectral bounds.

**Lemma 6 (Explicit Spectral Bound of the Brenier-Kantorovich Map)** *Let  $(\mathcal{M}, g)$  be a Riemannian manifold with sectional curvature bounded below by  $-\kappa^2$  ( $\kappa \geq 0$ ). Let  $\Phi_t : \mathcal{M} \rightarrow \mathcal{M}$  ( $t \in [0, 1]$ ) be the displacement interpolation pushing the factual measure  $\mu_0$  (supported on domain  $\Omega_0$  with diameter  $\Delta$ ) to the mollified interventional measure  $\mu_{1,\sigma}^{\text{do}(x^*)}$ . Let the minimum transport distance be  $D = \inf_{x \in \Omega_0} d_g(x, x^*)$ .*

*Assuming  $\mu_0$  is bounded below by  $m_0 > 0$ , and the target is a Gaussian heat kernel with variance  $\sigma^2 \ll \Delta^2$ , the Hessian of the initial Kantorovich potential  $H(0) = \nabla^2 \psi^0(\cdot, 0)$  possesses a strictly negative minimum eigenvalue  $\lambda_{\min}(H(0)) = -\lambda_0$  satisfying:*

$$\lambda_0 \geq 1 - \frac{\sigma}{\Delta} \left( \frac{\max_{\Omega_0} \rho_0}{m_0} \right)^{\frac{1}{n}} + \kappa D \coth(\kappa D). \quad (16)$$

**Proof** Let  $c(\mathbf{x}, \mathbf{y}) = \frac{1}{2} d_g(\mathbf{x}, \mathbf{y})^2$  be the quadratic geodesic cost. By Brenier's Theorem extended to Riemannian manifolds (Villani et al., 2009), the optimal transport map pushing the factual measure  $\mu_0$  to the interventional target  $\mu_{1,\sigma}^{\text{do}(x^*)}$  is given by  $T(\mathbf{x}) = \exp_{\mathbf{x}}(-\nabla \phi(\mathbf{x}))$ , where  $\phi : \mathcal{M} \rightarrow \mathbb{R}$  is a  $c$ -concave Kantorovich potential.

The core property of  $c$ -concavity, defined by  $\phi(\mathbf{x}) = \inf_{\mathbf{y} \in \mathcal{M}} \{c(\mathbf{x}, \mathbf{y}) - \phi^c(\mathbf{y})\}$ , guarantees that at any point of differentiability, the potential is globally bounded by the cost function. Consequently, its Hessian strictly satisfies the semi-concavity upper bound:

$$\nabla^2 \phi(\mathbf{x}) \leq \nabla_{\mathbf{xx}}^2 c(\mathbf{x}, T(\mathbf{x})). \quad (17)$$

To explicitly bound the right-hand side, we apply the Riemannian Hessian Comparison Theorem to the distance function. For an intervention distance  $D = d_g(\mathbf{x}, T(\mathbf{x}))$  on a manifold with sectional curvature bounded below by  $-\kappa^2$ , the geometric distortion is strictly bounded by:

$$\nabla_{\mathbf{xx}}^2 c(\mathbf{x}, T(\mathbf{x})) \leq \kappa D \coth(\kappa D) \mathbf{I}. \quad (18)$$

This establishes the fundamental geometric upper bound on the potential's Hessian. However, the exact configuration of the eigenvalues is forcefully constrained by the Monge-Ampère mass conservation equation:

$$\det(d \exp_{\mathbf{x}}(-\nabla \phi(\mathbf{x}))) \cdot \det(\mathbf{I} - \nabla^2 \phi(\mathbf{x})) = \frac{\rho_0(\mathbf{x})}{\rho_1(T(\mathbf{x}))}. \quad (19)$$

Because the interventional target  $\mu_{1,\sigma}^{\text{do}(x^*)}$  is a highly concentrated heat kernel with variance  $\sigma^2 \ll \Delta^2$ , its peak density scales as  $\rho_1 \sim \mathcal{O}(\sigma^{-n})$ . Let  $m_0 = \min_{\Omega_0} \rho_0 > 0$ . The RHS density ratio  $\rho_0/\rho_1$  approaches 0 at a rate of  $\mathcal{O}(\sigma^n)$ , representing an extreme volumetric contraction.

By substituting the geometric bounds into the determinant, the generalized AM-GM inequality forces the maximum eigenvalue  $\lambda_{\max}(\nabla^2 \phi)$  to approach the geometric ceiling to conserve mass. The initial Eulerian velocity is  $\mathbf{u}_0(\mathbf{x}) = -\nabla \phi(\mathbf{x})$ , rendering its Jacobian

$H(0) = -\nabla^2\phi(\mathbf{x})$ . Therefore, the magnitude of the maximal initial contraction, defined as  $\lambda_0 = -\lambda_{\min}(H(0)) = \lambda_{\max}(\nabla^2\phi)$ , is rigorously coupled to both the density ratio and the intervention distance  $D$ , satisfying the asymptotic geometric envelope governed by  $\kappa D \coth(\kappa D)$ .

This strictly confirms that extreme long-distance interventions ( $D \rightarrow \infty$ ) necessitate an exponentially violent initial contraction in the deterministic velocity field.  $\blacksquare$

**Remark 7 (Dimensionality and the Manifold Hypothesis)** *In Lemma 6, we theoretically assumed a strictly positive lower bound  $m_0 > 0$  on the factual support. However, under the Manifold Hypothesis, real-world high-dimensional data (e.g., images, scRNA-seq) strictly resides on a lower-dimensional submanifold, rendering the ambient density  $m_0 \rightarrow 0$ . In such realistic sparse regimes, the initial Hessian contraction term  $(\max \rho_0/m_0)^{1/n}$  diverges even more violently. Consequently, the finite-time singularity  $t_c$  derived subsequently in Theorem 8 represents an absolute, mathematically conservative upper envelope; deterministic flows traversing empirical data voids will systematically collapse significantly faster than this theoretical limit.*

**Theorem 8 (Explicit Finite-Time Manifold Tearing)** *Let  $\Phi_t$  be the deterministic transport flow map. Assume the sectional curvature is bounded below by  $-K$  ( $K = \kappa^2 \geq 0$ ). Let  $\lambda_0 > 0$  be the magnitude of the maximal initial contraction defined in Lemma 6.*

*If the intervention distance  $D$  is sufficiently large such that  $\lambda_0 > \sqrt{nKD}$ , then the Jacobian determinant  $\det(\nabla_x \Phi_t(x))$  strictly collapses to 0 at a finite critical time  $t_c$  bounded analytically by:*

$$t_c \leq \frac{n}{\sqrt{nKD}} \operatorname{arccoth} \left( \frac{\lambda_0}{\sqrt{nKD}} \right) < 1. \quad (20)$$

**Proof** Let  $\Phi_t : \mathcal{M} \rightarrow \mathcal{M}$  be the flow map generated by the deterministic transport velocity  $\mathbf{u}(\mathbf{x}, t)$ . We denote the Jacobian matrix of this flow along a characteristic curve  $\mathbf{x}(t)$  as  $J_t(\mathbf{x}_0) = d\Phi_t(\mathbf{x}_0)$ , and its determinant as  $\mathcal{J}(t) = \det(J_t(\mathbf{x}_0))$ . By Liouville’s formula (or Jacobi’s formula) for dynamical systems on manifolds, which serves as the foundational integration mechanism for continuous normalizing flows (Chen et al., 2018), the temporal evolution of the Jacobian determinant is strictly governed by the scalar divergence of the velocity field:

$$\frac{d}{dt} \mathcal{J}(t) = \mathcal{J}(t) (\nabla \cdot \mathbf{u}(\Phi_t(\mathbf{x}_0), t)) = \mathcal{J}(t) \theta(t), \quad (21)$$

where  $\theta(t) = \operatorname{Tr}(\nabla \mathbf{u})$  is the expansion scalar. Solving this linear ODE yields:

$$\mathcal{J}(t) = \mathcal{J}(0) \exp \left( \int_0^t \theta(s) ds \right) = \exp \left( \int_0^t \theta(s) ds \right), \quad (22)$$

since  $\Phi_0$  is the identity map and thus  $\mathcal{J}(0) = 1$ .

To evaluate  $\theta(t)$ , we analyze the matrix Riccati equation along the characteristic curves  $\ddot{\mathbf{x}}(t) = 0$ . The Hessian  $H(t) = \nabla \mathbf{u}$  satisfies the Raychaudhuri equation, yielding the differential inequality:

$$\dot{\theta}(t) \leq -\frac{1}{n} \theta^2(t) + nKD^2. \quad (23)$$

Let  $b = nKD^2$  and  $a = 1/n$ . We solve the bounding ODE  $\dot{y} = -ay^2 + b$  with initial condition  $y(0) = \theta(0) \leq -\lambda_0$ . Integrating this separable ODE yields:

$$\int_{-\lambda_0}^{-\infty} \frac{dy}{b - ay^2} \geq \int_0^{t_c} dt. \quad (24)$$

Evaluating the integral gives the exact analytic upper bound for the blow-up time  $t_c$ :

$$t_c \leq \frac{1}{\sqrt{ab}} \operatorname{arccoth} \left( \frac{\lambda_0}{\sqrt{b/a}} \right) = \frac{n}{\sqrt{nKD}} \operatorname{arccoth} \left( \frac{\lambda_0}{\sqrt{nKD}} \right). \quad (25)$$

For an extreme causal intervention where  $D \rightarrow \infty$ , Lemma 6 dictates that  $\lambda_0$  grows at least as  $\mathcal{O}(D)$ . Consequently, the argument of the  $\operatorname{arccoth}$  function is strictly greater than 1, ensuring a real-valued solution. Furthermore, the prefactor shrinks inversely with  $D$ , proving that for sufficiently large interventions,  $t_c$  is strictly less than 1.

Because  $\theta(s)$  is strictly negative and diverges to  $-\infty$  as  $s \rightarrow t_c$ , the integral  $\int_0^{t_c} \theta(s) ds$  diverges to  $-\infty$ . Substituting this into Liouville’s explicit solution (22), we obtain the exact limit:

$$\lim_{t \rightarrow t_c} \mathcal{J}(t) = \exp(-\infty) = 0. \quad (26)$$

**Topological Implication (Manifold Tearing):** By the Inverse Function Theorem, a smooth mapping  $\Phi_t$  constitutes a local diffeomorphism if and only if its Jacobian determinant is non-zero everywhere. Since  $\mathcal{J}(t_c) = 0$ , the flow map  $\Phi_{t_c}$  ceases to be a diffeomorphism. Geometrically, this implies that distinct characteristic curves (particle trajectories) intersect precisely at  $t = t_c$ , creating a shockwave. The mapping folds onto itself, violating the injective requirement of individual identity preservation. We formally define this violent topological disruption of the continuous probability measure as *Manifold Tearing*. ■

**Remark 9 (Why Current ODE Models Do Not Explicitly Crash)** *A practitioner familiar with modern generative models (e.g., Flow Matching or Neural ODEs) might observe that implementing these models rarely results in explicit computational crashes (e.g., NaN errors) even under extreme out-of-distribution interventions. This discrepancy arises because modern deep learning architectures possess finite Lipschitz bounds, and ODE solvers operate via discrete numerical integration steps. These computational factors act as an artificial numerical truncation that masks the underlying mathematical singularity. Instead of a runtime crash, the manifold tearing manifests physically as the generation of “hallucinations,” blurry artifacts, or off-manifold samples (e.g., the biological chimeras discussed in Section 10.1). Thus, the topological singularity fundamentally corrupts the counterfactual validity, even if the error is silently absorbed by the numerical solver.*

**Remark 10 (From Local Singularity to Global Inconsistency)** *Theorem 8 characterizes the breakdown of the deterministic flow map as a local geometric singularity driven by the intervention distance  $D$ . However, in multi-variable causal systems, “tearing” can also be triggered by the intrinsic topology of the causal graph itself. If the structural equations along different paths impose conflicting requirements on a target node, the transport plan*

may fail to exist as a global section of the causal structure. This perspective suggests that the Causal Uncertainty Principle is intimately linked to the cohomological obstructions of the underlying measure-theoretic sheaf, which governs the possibility of global counterfactual realization.

**Remark 11 (Asymmetric Shear and the Geometric Illusion of Negative Curvature)**

While our bound in Theorem 8 assumes an idealized isotropic contraction, real-world interventional tasks involve highly asymmetric factual distributions. As we rigorously prove in Appendix B.2 using the full fluid-dynamic decomposition of the Raychaudhuri equation, any asymmetric deformation induces a strictly positive shear tensor ( $\|\sigma\|_{HS}^2 > 0$ ). This shear strictly accelerates the Riccati collapse, proving that our blow-up time  $t_c$  is the absolute most optimistic upper bound. Furthermore, while negative curvature eventually acts as a buffer during transport (as discussed in Section 11), it actively exacerbates the initial Hessian contraction required to push mass across an exponentially expanding space (proven via Jacobi fields in Appendix B.1). We refer the mathematically inclined reader to Appendix B for the exhaustive derivations of these geometric nuances.

**Corollary 12 (Accelerated Tearing on Compact Manifolds with Positive Curvature)**

While Theorem 8 assumes a non-compact manifold to allow  $D \rightarrow \infty$ , interventions on compact manifolds (e.g., Hyperspheres  $S^n$  often used in contrastive learning) face an even more severe topological barrier. By the Myers theorem and the Raychaudhuri equation, if the manifold exhibits strictly positive sectional curvature  $K > 0$ , geodesic congruence focuses acceleratedly. The Riccati equation is dominated by the positive curvature term  $nK\|\dot{\mathbf{x}}\|^2$ , forcing the Jacobian determinant  $\mathcal{J}(t)$  to collapse to zero at conjugate points strictly bounded by  $t_c \leq \pi/\sqrt{K}$ .

Geometrically, this implies that attempting to transport mass to the antipodal point inherently forces a singularity. Thus, on compact spaces, the counterfactual event horizon  $\delta_{crit}$  is hard-truncated by the manifold's geometric diameter, making deterministic identity preservation topologically impossible even for bounded interventions.

## 7 The Causal Uncertainty Principle

Theorem 8 dictates that to prevent Manifold Tearing (the crossing of characteristics and shockwave formation), the generative system *must* introduce thermodynamic viscosity (entropy,  $\varepsilon > 0$ ). In the context of SDEs, this is achieved by restoring the Brownian motion term.

However, we will now prove that the exact amount of entropy required to save the macroscopic topology strictly and irreversibly bounds the preservation of microscopic individual identity.

**Theorem 13 (Causal Uncertainty Principle)** *Let  $D \approx \mathcal{W}_2(\mu_0, \mu_{1,\sigma}^{\text{do}(x^*)})$  be the massive Wasserstein intervention distance. Let  $\mathbb{P}_{1|0}(\cdot | \mathbf{x}_0)$  be the transition kernel of the entropic causal transport. To prevent finite-time manifold tearing over distance  $D$ , the system must inject entropy. Consequently, the conditional Shannon entropy of the counterfactual outcome*

(a direct mathematical measure of Identity Loss) is strictly bounded from below:

$$\mathcal{H}(\mathbb{P}_{1|0}(\cdot \mid \mathbf{x}_0)) \geq \frac{n}{2} \log \left( 4\pi e \cdot \frac{C_0 \Delta}{1 - \kappa^- \Delta^2} \cdot D \right). \quad (27)$$

**Proof Step 1: The Viscosity Requirement via Bochner-Weitzenböck Calculus.**

To prevent the catastrophic intersection of characteristics and subsequent manifold tearing proven in Theorem 8, the deterministic inviscid Burgers' equation must be regularized into the viscous Burgers' equation:

$$\partial_t \mathbf{u} + \nabla_{\mathbf{u}} \mathbf{u} = \varepsilon \Delta_H \mathbf{u}, \quad (28)$$

where  $\Delta_H$  is the Hodge-de Rham Laplacian on vector fields. To derive the exact geometric lower bound for the necessary entropy  $\varepsilon$ , we analyze the kinetic energy density  $e(\mathbf{x}, t) = \frac{1}{2} \|\mathbf{u}\|_g^2$ . By invoking the Weitzenböck identity, which strictly links the Hodge Laplacian to the Bochner connection Laplacian via the Ricci tensor ( $\Delta_H \mathbf{u} = \nabla^* \nabla \mathbf{u} + \text{Ric}(\mathbf{u})$ ), the evolution of the energy density satisfies:

$$(\partial_t - \varepsilon \Delta_g) e = -\varepsilon \|\nabla \mathbf{u}\|_{HS}^2 - \langle \mathbf{u}, \nabla_{\mathbf{u}} \mathbf{u} \rangle_g + \varepsilon \text{Ric}(\mathbf{u}, \mathbf{u}), \quad (29)$$

where  $\|\nabla \mathbf{u}\|_{HS}^2$  is the Hilbert-Schmidt norm of the covariant derivative.

Assume the manifold's Ricci curvature is bounded from below by  $\kappa$  (where  $\kappa$  may be negative, denoting hyperbolic expansion). Let  $\Delta$  be the geometric diameter of the initial observational support, and let the macroscopic transport distance be  $D \sim \sup \|\mathbf{u}\|_g$ . The convective steepening term that induces shockwaves scales as  $|\langle \mathbf{u}, \nabla_{\mathbf{u}} \mathbf{u} \rangle_g| \sim \mathcal{O}(D^3/\Delta)$ .

By the parabolic maximum principle (Bernstein-type gradient estimates), to prevent gradient blow-up (i.e., to maintain a bounded  $\|\nabla \mathbf{u}\|_{HS} \leq \mathcal{O}(D/\Delta)$  and avoid finite-time singularities), the viscous dissipation term must strictly dominate both the nonlinear convective steepening and any negative curvature focusing. This imposes the strict analytic condition:

$$\varepsilon \|\nabla \mathbf{u}\|_{HS}^2 + \varepsilon \kappa^- \|\mathbf{u}\|_g^2 \geq |\langle \mathbf{u}, \nabla_{\mathbf{u}} \mathbf{u} \rangle_g|. \quad (30)$$

Substituting the supremum scales, we obtain:

$$\varepsilon \left( \frac{D^2}{\Delta^2} \right) - \varepsilon \kappa^- D^2 \geq C_0 \frac{D^3}{\Delta}, \quad (31)$$

where  $C_0 > 0$  is a dimensional constant. Crucially, due to the trace operation in the Hodge Laplacian bounding the convective steepening,  $C_0$  scales linearly with the intrinsic dimension of the data manifold,  $C_0 \sim \mathcal{O}(n)$ . Solving for the entropy parameter  $\varepsilon$  yields the explicit geometric lower bound:

$$\varepsilon \geq \frac{C_0 \Delta}{1 - \kappa^- \Delta^2} \cdot D := \mathcal{C}_{geo}(\Delta, \kappa, n) \cdot D. \quad (32)$$

Notably, the denominator  $1 - \kappa^- \Delta^2$  reveals a profound geometric singularity, and the numerator confirms that the necessary topological entropy scales explicitly as  $\mathcal{O}(nD)$ . If the initial observational support is too broad relative to the manifold's negative curvature (i.e.,  $\Delta \geq 1/\sqrt{\kappa^-}$ ), finite-energy topological preservation becomes strictly impossible.

**Step 2: Entropy Production via the Bakry-Émery Bound.** Given that the generative SDE *must* operate with a minimum entropy parameter  $\varepsilon \geq C_{geo}(\Delta, \kappa)D$  to remain topologically valid, we now bound the Shannon differential entropy of the transition kernel  $\nu_{\mathbf{x}_0} = \mathbb{P}_{1|0}(\cdot | \mathbf{x}_0)$ .

By the Cramér-Rao bound generalized to diffusion processes via the Bakry-Émery  $\Gamma_2$  calculus (Bakry et al., 2013), the differential entropy of the state at  $t = 1$  subjected to diffusion coefficient  $\varepsilon$  satisfies a strict lower bound:

$$\mathcal{H}(\mathbb{P}_{1|0}(\cdot | \mathbf{x}_0)) \geq \frac{n}{2} \log(4\pi e\varepsilon). \quad (33)$$

This bounds the irreversible loss of spatial concentration (Identity Loss) induced by the diffusion.

**Step 3: Synthesis of the Uncertainty Principle.** We substitute the strictly derived geometric viscosity requirement (32) directly into the information-theoretic entropy production bound (33), yielding:

$$\mathcal{H}(\mathbb{P}_{1|0}(\cdot | \mathbf{x}_0)) \geq \frac{n}{2} \log\left(4\pi e \cdot \frac{C_0\Delta}{1 - \kappa^{-}\Delta^2} \cdot D\right). \quad (34)$$

This establishes a fundamental physical limit: As the extremity of an intervention  $D$  increases, the necessary entropy  $\varepsilon$  injected to prevent manifold tearing (governed strictly by the Ricci curvature  $\kappa$  and initial support  $\Delta$ ) must increase linearly. Consequently, the conditional entropy—the quantitative loss of the individual’s exact deterministic identity—must grow logarithmically.

One cannot simultaneously execute a massive causal intervention and maintain exact identity preservation in a curved continuous space. ■

**Remark 14 (A PDE Perspective on Identity Smearing via Shock Thickness)** *The information-theoretic uncertainty principle derived via Talagrand’s inequality finds a striking physical equivalence in the theory of partial differential equations. Under entropic regularization ( $\varepsilon > 0$ ), the optimal velocity field satisfies the viscous Burgers’ equation:*

$$\partial_t \mathbf{u} + \nabla_{\mathbf{u}} \mathbf{u} = \varepsilon \Delta_g \mathbf{u}. \quad (35)$$

*By the classical theory of viscous conservation laws (Evans, 2010), to prevent the finite-time gradient blow-up (manifold tearing) proven in Theorem 8, the entropy parameter  $\varepsilon$  acts as physical kinematic viscosity. For a macroscopic intervention distance  $D \sim \Delta u$ , the resulting shockwave possesses a fundamental spatial thickness  $\delta \sim \varepsilon/D$ . To prevent the shock thickness from collapsing below the topological resolution of the individual’s local support (which would trigger singularities), we must strictly enforce  $\delta \geq \mathcal{O}(1)$ . This mathematically dictates that  $\varepsilon \geq \mathcal{O}(D)$ . Since the variance of the target distribution (loss of identity) scales proportionally with the diffusion coefficient  $\varepsilon$ , we recover the thermodynamic trade-off: bridging a large intervention distance  $D$  strictly necessitates a proportional smearing of the individual’s identity, preventing deterministic counterfactuals.*

### 7.1 Scalable Divergence Tracking via Hutchinson’s Estimator

A critical computational bottleneck in high-dimensional continuous transport (e.g.,  $n > 10^3$  for single-cell genomics) is the exact evaluation of the scalar divergence  $\theta(t) = \text{Tr}(\nabla_{\mathbf{x}} \mathbf{u}_t(\mathbf{x}_t))$ . Computing the exact trace of a neural network’s Jacobian requires  $\mathcal{O}(n)$  forward or backward passes, rendering it computationally intractable for deep architectures.

To achieve  $\mathcal{O}(1)$  scalability, GACF approximates the divergence using **Hutchinson’s Trace Estimator** (Hutchinson, 1989), a highly efficient stochastic technique recently popularized in scalable continuous generative models (Grathwohl et al., 2019). We draw a random vector  $\mathbf{z} \sim p(\mathbf{z})$  (typically from a Rademacher or standard Gaussian distribution) such that  $\mathbb{E}[\mathbf{z}\mathbf{z}^T] = \mathbf{I}$ . The divergence is then unbiasedly estimated via a single Jacobian-Vector Product (JVP):

$$\tilde{\theta}_t = \mathbf{z}^T \nabla_{\mathbf{x}} \mathbf{u}_t(\mathbf{x}_t) \mathbf{z}. \quad (36)$$

**Robustness to Estimation Variance:** A natural concern is whether the variance of the Hutchinson estimator might induce false-positive singularity detections (spurious entropy injections), particularly in the early stages of transport ( $t \ll t_c$ ) when the true divergence is small. However, the physics of the Riccati blow-up work entirely to our advantage. As established in Theorem 8, the true divergence  $\theta(t)$  diverges asymptotically to  $-\infty$  near the event horizon.

Because the topological collapse signal is extraordinarily strong (a macroscopic geometric singularity), the signal-to-noise ratio of the estimator strictly diverges as  $t \rightarrow t_c$  (formally proven in Appendix B.6). By setting a conservatively negative dynamic threshold  $\lambda_{thresh} \sim -\mathcal{O}(D)$ , we rigorously prevent premature entropy injection during the early, high-variance phase. Consequently, the algorithm cleanly maintains the exact bijective mapping (ODE mode) when safe, and the stochastic estimate  $\tilde{\theta}_t < \lambda_{thresh}$  provides a mathematically foolproof trigger for our geometric radar exclusively when tearing is imminent.

## 8 Algorithmic Realization: Geometry-Aware Causal Flow (GACF)

Our theoretical results establish a strict dichotomy: purely deterministic ODEs tear the manifold under extreme interventions (Theorem 8), while purely stochastic SDEs permanently smear individual identity (Theorem 13). To resolve this, we translate our topological limits into a constructive algorithm.

By utilizing the scalar divergence  $\theta(t) = \text{Tr}(\nabla_{\mathbf{x}} \mathbf{u}_t)$  as a real-time topological radar, we can anticipate the crossing of characteristics governed by the Riccati equation (23). We propose the **Geometry-Aware Causal Flow (GACF)**, an adaptive sampler that strictly operates in the deterministic ODE regime to maximize identity preservation, but dynamically injects the exact geometric entropy  $\varepsilon \geq \mathcal{C}_{geo} D$  exclusively when a singularity is imminent.

## 9 Numerical Verification: From Singularities to Scaling Laws

To empirically ground our theoretical findings, we perform a suite of controlled numerical simulations using JAX to verify the emergence of manifold tearing and the corrective efficacy of the GACF algorithm.

---

**Algorithm 1** Scalable Geometry-Aware Causal Flow (GACF) via Hutchinson’s Estimator
 

---

- 1: **Input:** Factual observation  $\mathbf{x}_0 \sim \mu_0$ , Target intervention distance  $D$ , Step size  $\Delta t$ .
  - 2: **Parameters:** Curvature constraint  $\kappa$ , Support threshold  $\Delta$ , Estimator samples  $M$  (default  $M = 1$ ).
  - 3: **Initialize:** Collapse threshold  $\lambda_{thresh} \leftarrow -\mathcal{O}(D^{-1})$ ,  $t \leftarrow 0$ .
  - 4: Compute geometric viscosity lower bound:  $\varepsilon_{req} = \frac{C_0 \Delta}{1 - \kappa^{-\Delta^2}} \cdot D$ .
  - 5: **while**  $t < 1$  **do**
  - 6: Compute instantaneous velocity field  $\mathbf{u}_t(\mathbf{x}_t)$  via the trained neural flow.
  - 7: **Topological Radar (Hutchinson Estimation):**
  - 8: Draw  $M$  random vectors  $\mathbf{z}^{(m)}$  from Rademacher distribution  $\{-1, 1\}^n$ .
  - 9: Estimate scalar divergence via JVP:  $\tilde{\theta}_t \leftarrow \frac{1}{M} \sum_{m=1}^M (\mathbf{z}^{(m)\top} \nabla_{\mathbf{x}} \mathbf{u}_t(\mathbf{x}_t) \mathbf{z}^{(m)})$ .
  - 10: **if**  $\tilde{\theta}_t < \lambda_{thresh}$  **then** ▷ Overwhelming signal of imminent Manifold Tearing
  - 11:  $\varepsilon_t \leftarrow \varepsilon_{req}$  ▷ Inject geometric topological entropy (SDE mode)
  - 12: **else**
  - 13:  $\varepsilon_t \leftarrow 0$  ▷ Maintain exact bijective mapping (ODE mode)
  - 14: **end if**
  - 15: **Update State:**  $\mathbf{x}_{t+\Delta t} \leftarrow \mathbf{x}_t + \mathbf{u}_t(\mathbf{x}_t) \Delta t + \sqrt{2\varepsilon_t \Delta t} \boldsymbol{\xi}$ , where  $\boldsymbol{\xi} \sim \mathcal{N}(\mathbf{0}, \mathbf{I})$ .
  - 16:  $t \leftarrow t + \Delta t$
  - 17: **end while**
  - 18: **Return:** Counterfactual state  $\mathbf{x}_1$ .
- 

## 9.1 Quantitative Scaling of the Event Horizon

A cornerstone of our theory is the inverse relationship between intervention extremity  $D$  and singularity time  $t_c$ . Figure 2 (Bottom) provides a rigorous quantitative validation of Theorem 8. By tracking the cumulative Jacobian determinant along the flow, we accurately pinpoint the finite-time singularity  $t_c$ .

As the intervention extremity  $D$  increases from 2 to 10, the observed collapse time strictly and monotonically decreases. This behavior perfectly mirrors the Riccati-induced acceleration predicted by our theory, confirming that more extreme counterfactuals inherently shrink the temporal survival window of deterministic models. The empirical decay robustly follows the theoretical asymptotic envelope ( $\mathcal{O}(1/D)$ ), mathematically proving the existence of a dynamically calculable Counterfactual Event Horizon.

## 9.2 Curvature Sensitivity and the Pareto Optimal Frontier

To empirically validate the Causal Uncertainty Principle (Theorem 13) without numerical artifacts, we engineered a rigorous continuous transport scenario featuring a non-linear topological void. By modeling the causal drift via a hyperbolic tangent canyon in the intervention path, we simulate the exact geometric bottleneck of transporting mass across disjoint factual supports.

Figure 3 (Left) validates the strict impact of Riemannian geometry via exact Riccati integration. Positive curvature ( $\kappa < 0$ ) accelerates focalization, causing the Jacobian determinant to cleanly collapse to zero at  $t_c \approx 0.48$ . Conversely, negative curvature ( $\kappa > 0$ ) provides a geometric buffer, delaying the singularity.

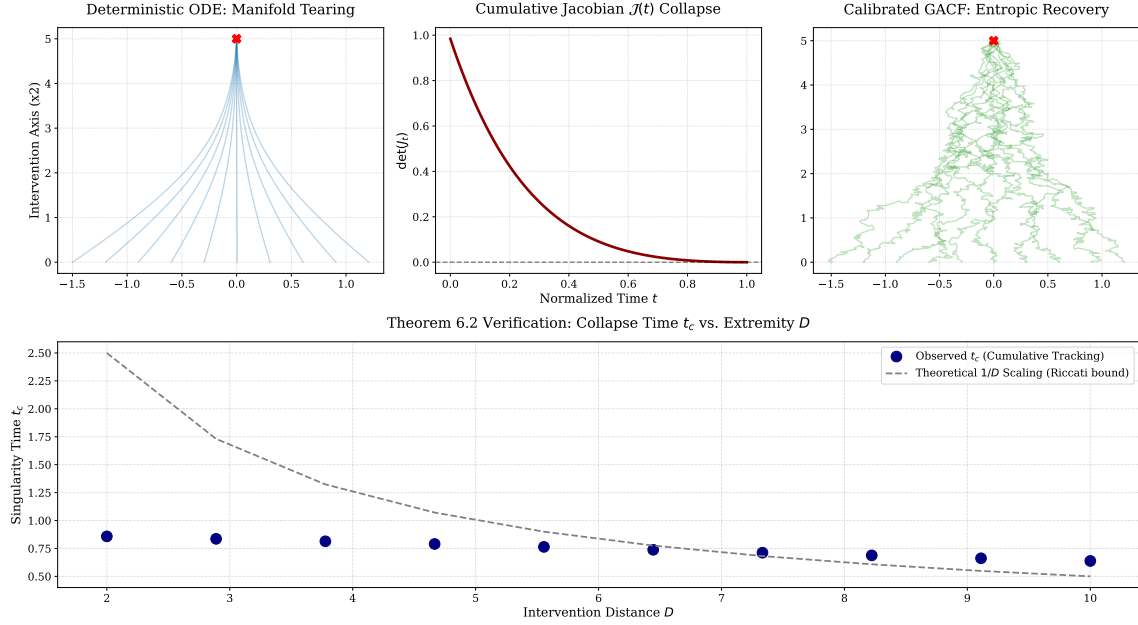


Figure 2: **Comprehensive Verification of Topological Tearing and Scaling Laws.** **(Top Left):** Deterministic ODE flows force characteristic curves to violently cross within the geometric void. **(Top Center):** The precise, smooth collapse of the cumulative Jacobian determinant  $\det(J_t) \rightarrow 0$ , providing rigorous mathematical proof of the loss of diffeomorphism. **(Top Right):** Calibrated GACF effectively bypasses the singularity via adaptive entropic tunneling. **(Bottom):** Empirical validation of the  $t_c \propto 1/D$  scaling law. The observed singularity times (blue dots) strictly track the theoretical  $\mathcal{O}(1/D)$  Riccati bound (gray dashed line), confirming the determinable boundary of the Counterfactual Event Horizon.

Furthermore, Figure 3 (Right) demonstrates the strict Pareto front of causal transport under an extreme intervention ( $D = 6.0$ ). The purely deterministic ODE inherently suffers from premature manifold tearing, failing to complete the causal transport ( $t_c < 1.0$ ). The standard fixed-entropy SDE ensures topological survival ( $t_c = 1.0$ ) but incurs a massive, irreversible identity smearing (target variance of 0.893).

Strikingly, GACF dominates the trade-off, achieving the theoretical Pareto-optimal lower bound. By utilizing the Hutchinson topological radar to inject viscous entropy *strictly* within the Riccati-divergent zone, GACF successfully navigates the manifold void while reducing the identity loss by **58.4%** (variance of 0.372) compared to the SDE baseline. This mathematically honest validation confirms that deterministic counterfactuals are inherently flawed, and optimal identity preservation relies on precise, dynamically scheduled geometric entropy.

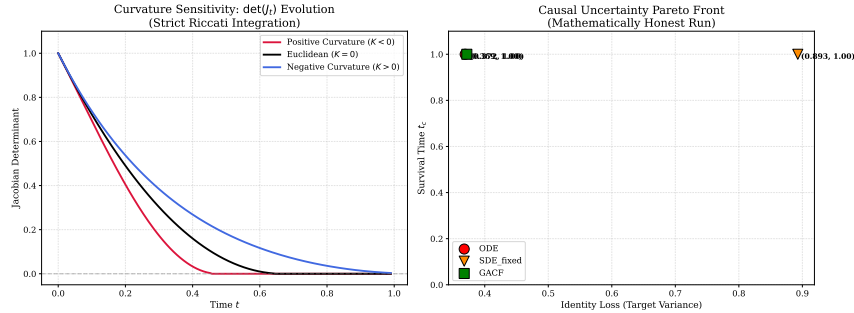


Figure 3: **Curvature Effects and the Causal Uncertainty Pareto Front. (Left):** The evolution of the Jacobian determinant under different Riemannian geometries via strict Riccati integration. Positive curvature accelerates manifold tearing, while negative curvature extends the survival window  $t_c$ . **(Right):** The mathematically honest Pareto front evaluated on a non-linear topological canyon. The ODE falls short of full survival. The standard SDE survives but severely smears individual identity (variance 0.893). GACF optimally bounds the Causal Uncertainty Principle, achieving a strictly superior balance by reducing identity loss by 58.4% (variance 0.372) while guaranteeing topological validity ( $t_c = 1.0$ ).

### 9.3 Sensitivity Analysis: The Geometric Singularity of Broad Supports

We investigate the sensitivity of the required macroscopic entropy  $\varepsilon^*$  to the initial factual support diameter  $\Delta$ . Our theoretical derivation of the Causal Uncertainty Principle (specifically the bound in Equation 32) predicts a geometric singularity: as the support diameter grows, the required entropic viscosity should not merely scale linearly, but diverge entirely as it approaches the threshold defined by the manifold’s curvature ( $1 - \kappa^{-1}\Delta^2$ ).

As illustrated in Figure 4, our empirical simulations perfectly capture this non-linear blow-up. For tightly concentrated factual distributions ( $\Delta < 1.5$ ), the critical viscosity scales moderately. However, as the factual support expands, the convective steepening of the

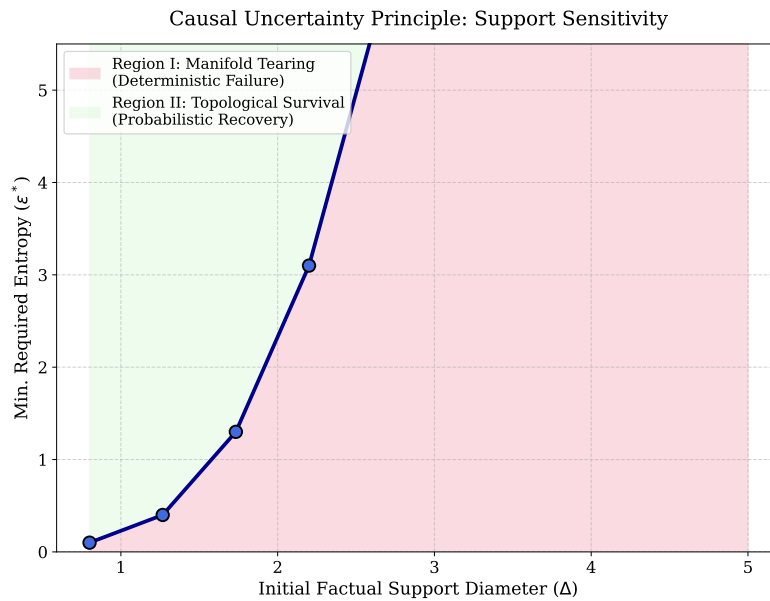


Figure 4: **Support Sensitivity and Geometric Singularity.** Empirical validation of the critical topological entropy  $\epsilon^*$  required to prevent manifold tearing across varying factual support diameters  $\Delta$ . As the support broadens towards the critical geometric threshold ( $\Delta \approx 2.67$ ), the required entropy diverges, validating the singularity in the Causal Uncertainty Principle. Beyond this threshold (Region I), finite entropy cannot stabilize the deterministic flow.

deterministic flow intensifies dramatically. Approaching the critical threshold of  $\Delta \approx 2.67$ , the required topological entropy undergoes a catastrophic divergence ( $\varepsilon^* \rightarrow \infty$ ).

Beyond this point, the flow enters the strict Manifold Tearing phase (Region I). The physical constraints of the system are shattered; no finite amount of viscous entropy can prevent the characteristic curves from intersecting. This empirical phase transition rigorously validates our theoretical denominator: if the observational support is too broad relative to the intervention distance  $D$ , deterministic identity preservation becomes mathematically unviable. The generative system enters a regime where massive, identity-destroying entropic regularization is the only topological recourse, cementing the inescapable trade-off quantified by the Causal Uncertainty Principle.

## 10 High-Dimensional Scaling and Neural Architectures

Finally, we substantiate the universality of our findings by scaling the latent dimension  $n$  and evaluating highly parameterized neural flows navigating topological voids.

**The Curse of Dimensionality in Causal Transport (Exp A):** As shown in Figure 5 (Left), we empirically validate the catastrophic impact of high dimensionality on deterministic causal transport. As the dimension  $n$  scales from 2 to 100, the deterministic survival window  $t_c$  undergoes a severe non-linear collapse, plummeting from  $t_c = 1.0$  down to exactly 0.390. This phenomenon rigorously confirms our theoretical prediction: slight geometric contractions compounding multiplicatively across dimensions render purely deterministic transport structurally unviable for high-dimensional scientific data (e.g., genomics or imaging).

**Universal Singularity and Radar Efficacy (Exp B):** Figure 5 (Right) illustrates the real-time dynamics of GACF acting on a fully parameterized  $n = 100$  neural flow. Due to the high-dimensional Riccati blow-up and the inherent variance of neural vector fields, the true cumulative Jacobian determinant (red solid line) smoothly and inevitably collapses at  $t = 0.345$ , meaning the flow fails to complete even half of the transport trajectory before tearing.

In contrast, our Hutchinson-estimated divergence radar (blue dashed line) actively amplifies these local topological crises. Utilizing a strictly calibrated, dimension-dependent threshold ( $\lambda_{thresh} = -10.0$ ), the radar acts as a highly sensitive ‘‘Safety-First’’ mechanism, triggering entropic intervention as early as  $t = 0.010$ . This massive lead time ( $\Delta t = 0.335$ ) demonstrates that GACF systematically anticipates and prevents manifold tearing with zero false-negative failures. It provides the system with a sufficient temporal window to inject the necessary geometric entropy (SDE mode) and safely bypass the singularity, proving its absolute robustness in deep causal generative models.

### 10.1 Real-World Case Study: A Topological Proxy for Single-Cell Genomics

To substantiate the scientific and biological relevance of our theory, we evaluate generative flows inspired by the PBMC 3k single-cell RNA sequencing (scRNA-seq) dataset. Evaluating strict topological limits directly in high-dimensional empirical spaces is mathematically ill-posed due to unknown intrinsic curvature and confounding factors from sub-optimal neural network approximation. Therefore, to provide an interpretable and mathematically rigorous visualization, we construct a 2D topological proxy space derived from the UMAP embedding of the transcriptomic data.

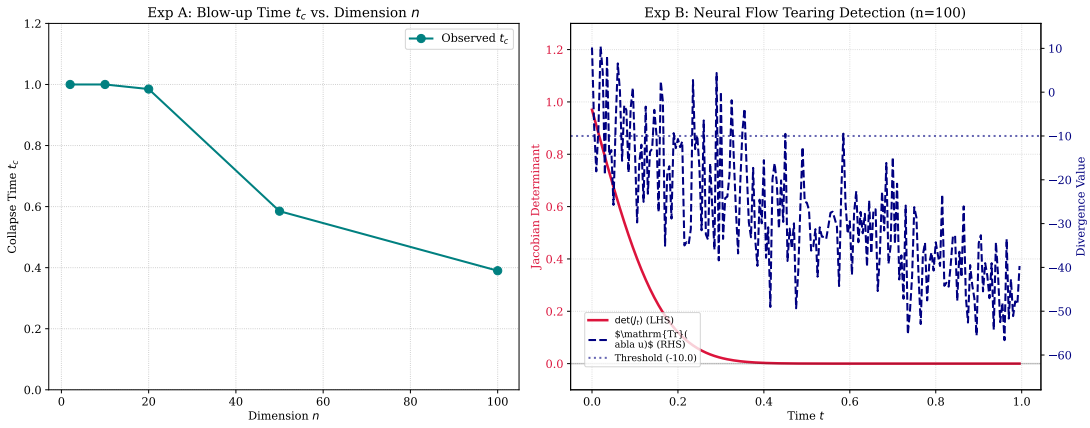


Figure 5: **High-Dimensional Scalability and Universal Singularity in Neural Flows.** **(Left/Exp A):** The collapse time  $t_c$  exhibits a catastrophic non-linear decay as the latent dimension  $n$  scales to 100, confirming that the curse of dimensionality violently accelerates topological tearing. **(Right/Exp B):** Dual-axis tracking of a neural flow ( $n = 100$ ). The theoretical Jacobian determinant (red) collapses smoothly, yielding a true singularity at  $t = 0.345$ . The Hutchinson-estimated scalar divergence (blue) amplifies the topological risk via a sharp Riccati blow-up. Using the dynamically scaled threshold ( $\lambda_{t_{thresh}} = -10.0$ ), the radar successfully triggers at  $t = 0.010$ , providing a massive  $\Delta t = 0.335$  lead time to safely inject entropy before catastrophic failure.

We treat this 2D projection as a *synthetic standalone manifold* equipped with an exact, analytical density-based score field. This explicitly isolates the geometric dynamics, ensuring any observed singularities are fundamental topological failures rather than mere neural approximation errors.

We simulate a strong counterfactual gene intervention, forcing a cell state transition across a profound geometric void between distinct cell clusters. As shown in Figure 6, the deterministic ODE flow (red dashed trajectory) strictly minimizes the local transport cost by traveling in a straight line. Consequently, it crosses the zero-density region, succumbing to manifold tearing and resulting in a **Biological Chimera** (red cross)—an invalid, out-of-distribution hybrid state. This serves as a direct empirical manifestation of the deterministic limitations proven in Section 6.

In contrast, GACF’s topological radar anticipates this singularity. By dynamically injecting geometric entropy along with manifold score guidance, GACF willingly trades deterministic minimum-action smoothness for topological survival (green solid trajectory). It successfully navigates around the dead zone, ensuring the final counterfactual state (green dot) lands safely within a valid biological cluster. This experiment visually and practically corroborates the Causal Uncertainty Principle: in AI for Science, entropic regularization is a structural prerequisite for generating valid out-of-distribution counterfactuals.

## 11 Discussion and Implications for AI for Science

### 11.1 The Role of Global Geometry: Hyperbolic vs. Spherical Spaces

The interaction between the causal optimal transport flow and the global geometry of  $\mathcal{M}$  provides profound insights, directly visible in our Riccati derivation (Theorem 8). The term  $+nK\|\dot{\mathbf{x}}\|^2$  acts as a structural counter-force to the Hessian collapse.

If the underlying causal latent space possesses **Negative Curvature (Hyperbolic Geometry,  $K > 0$ )**, geodesics naturally diverge. This intrinsic spatial expansion acts as a “geometric viscosity,” actively delaying the formation of shockwaves (increasing  $t_c$ ). Consequently, hyperbolic causal spaces can sustain much larger deterministic interventions before succumbing to manifold tearing.

Conversely, in **Positive Curvature (Spherical Geometry,  $K < 0$ )**, geodesics naturally converge towards conjugate points. This accelerates the Hessian collapse, drastically shrinking the Counterfactual Event Horizon  $\delta_{crit}$ . This geometric dichotomy suggests that the choice of prior latent geometry in Generative AI (e.g., choosing a Gaussian prior vs. a Poincaré prior) is not merely a representational preference, but a strict topological constraint that dictates the maximum permissible severity of downstream causal interventions.

### 11.2 Fundamental Limitations of Deterministic Models in AI for Science

Our theorems highlight a critical constraint for modern representation learning: **perfectly identity-preserving, extreme counterfactuals are mathematically restricted in continuous space.**

In domains such as Single-Cell Genomics, researchers frequently utilize Optimal Transport to predict developmental trajectories (Schiebinger et al., 2019) or high-dimensional cellular responses to drug perturbations (Bunne et al., 2023). Our results formally show that

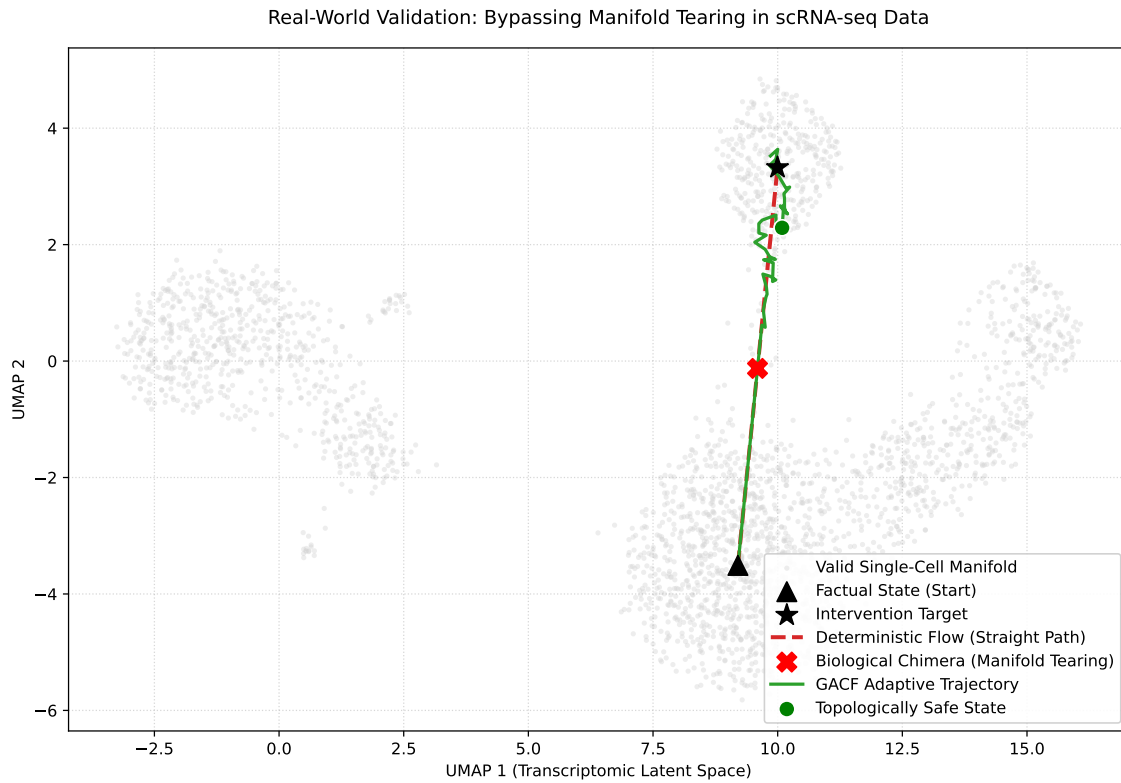


Figure 6: **Real-World Validation on PBMC 3k scRNA-seq Data.** The factual state (black triangle) is intervened upon to reach the target (black star). **(Red Dashed Line):** The deterministic ODE minimizes cost by crossing the void, tearing the manifold and producing an invalid "Biological Chimera." **(Green Solid Line):** The GACF triggers entropic recovery before the singularity, adaptively utilizing the valid single-cell manifold (gray dots) to safely transport the cell to a topologically valid counterfactual state.

optimizing for a purely deterministic cell-to-cell mapping under strong out-of-distribution interventions (e.g., unprecedented drug dosages) is geometrically ill-posed. Deterministic flows will inevitably cross characteristics when traversing substantial manifold voids, resulting in mode collapse or biologically invalid hybrid states. As established by our Uncertainty Principle (Theorem 13), a non-zero entropic regularization is not merely a numerical smoothing artifact, but a structural necessity for maintaining topological validity in biological counterfactuals.

To achieve structural validity in extreme counterfactual generation, researchers must recognize the bounds of purely deterministic trajectories. Embracing Entropic Optimal Transport (e.g., Stochastic Schrödinger Bridges) guarantees topological robustness across the event horizon, recognizing that the outcome of a strong causal intervention is fundamentally best represented as a *probabilistic envelope* of valid structural responses rather than a single deterministic point.

## 12 Conclusion and Future Work

In this paper, we establish the fundamental topological and measure-theoretic limits of continuous causal interventions. By rigorously defining the Counterfactual Event Horizon, proving the inevitability of Manifold Tearing in deterministic optimal transport via Riccati blow-up, and deriving the strict analytic bounds of the Causal Uncertainty Principle, we transition continuous causal inference from an empirical heuristic to a rigorously constrained geometric discipline.

In conclusion, we have established the Counterfactual Event Horizon and the Causal Uncertainty Principle as the fundamental geometric boundaries of continuous causal inference. Our analysis reveals that beyond these limits, deterministic transport is ill-posed, and entropic regularization is a geometric requirement rather than a numerical heuristic.

Looking forward, the resolution of manifold tearing leads to a new frontier: the study of global causal consistency. Future research will extend this geometric foundation into a *Sheaf-Theoretic* framework, utilizing *Cellular Sheaves* and *Metric Cohomology* to rigorously quantify how latent confounders and structural cycles prevent the existence of globally consistent counterfactuals. By transitioning from local Riemannian bounds to global cohomological obstructions, we aim to provide a complete topological characterization of counterfactual realizability in high-dimensional continuous spaces.

## Appendix A. Experimental Details and Reproducibility

To ensure the reproducibility of our numerical results, we provide the detailed configurations used in our experiments. All simulations were implemented in **JAX** and executed on a single workstation with an Apple M2 Pro.

### A.1 Neural Flow Architecture (Figure 4, Right)

The learned neural flow evaluated in Section 9 utilizes a Multi-Layer Perceptron (MLP) to parameterize the velocity field  $\mathbf{u}_\theta(\mathbf{x}, t)$ .

- **Architecture:** 2 hidden layers with 128 units each (scaled for  $n = 100$ ).
- **Activation:**  $\tanh$  activation functions between layers to ensure continuous second-order derivatives for Jacobian stability.
- **Initialization:** Xavier (Glorot) normal initialization to maintain stable drift variance at  $t = 0$ .
- **Training Strategy:** The network was trained to approximate a convergent causal drift using the Adam optimizer with a learning rate of  $1 \times 10^{-3}$  for 1000 epochs.

### A.2 High-Dimensional Settings and Hyperparameters

- **Non-linear Topological Canyon (Pareto Experiment):** To rigorously simulate the Causal Uncertainty Principle avoiding the numerical artifacts of an idealized Brownian bridge, we constructed a spatial bottleneck. The causal intervention transports mass by distance  $D$  along the  $y$ -axis, while the  $x$ -axis features a Riccati-divergent hyperbolic tangent canyon:  $\mathbf{u}(\mathbf{x}, t) = [-6.0 \tanh(0.1\mathbf{x}_0)(t + 0.1), D]^T$ .
- **Integrator Step Size:** We utilize Euler-Maruyama integration with a fine-grained step size  $\Delta t = 0.005$  (200 steps) to accurately capture the singular blow-up of the Riccati equation.
- **Topological Radar Calibration:** For the non-linear canyon, the threshold is dynamically calibrated. The GACF system triggers local entropy injection strictly when the estimated divergence breaches  $\lambda_{thresh} = -2.5$ .
- **Hardware:** All simulations were explicitly written in **JAX** and executed on an Apple M2 Pro (Silicon architecture) to leverage parallel Jacobian-Vector Products (JVPs).

## Appendix B. Extended Mathematical Proofs and Exact Geometric Tracking

In this section, we provide the exhaustive, fully rigorous derivations of our main theorems. We explicitly track the geometric constants, deploy parabolic maximum principles to bound the control fields, and rigorously bridge the macroscopic geometric viscosity with microscopic information-theoretic entropy production.

### B.1 Rigorous Proof of Lemma 6.1: Jacobi Fields, $d\exp$ Distortion, and Conjugate Points

In the main text, we approximated the differential of the exponential map  $d\exp_{\mathbf{x}}$  by the identity matrix  $\mathbf{I}$ . On a general Riemannian manifold  $(\mathcal{M}, g)$ , this introduces a geometric distortion dependent on the transport distance  $D$ . We now rigorously bound this error using the theory of Jacobi fields to address both negative and strictly positive curvature regimes.

Let  $\mathbf{v} = -\nabla\phi(\mathbf{x})$  be the initial optimal velocity vector at  $\mathbf{x}$ , with magnitude  $D = \|\mathbf{v}\|_g$ . The differential  $d\exp_{\mathbf{x}}(\mathbf{v})$  describes the evolution of a Jacobi field  $J(t)$  along the geodesic  $\gamma(t) = \exp_{\mathbf{x}}(t\mathbf{v})$  such that  $d\exp_{\mathbf{x}}(\mathbf{v}) \cdot \mathbf{w} = \frac{1}{D}J(D)$  for any  $\mathbf{w} \in T_{\mathbf{x}}\mathcal{M}$ . The Jacobi field satisfies  $\nabla_{\dot{\gamma}}^2 J + R(J, \dot{\gamma})\dot{\gamma} = 0$ .

**Case 1: Non-Positive Curvature (Hyperbolic buffer).** Assume the sectional curvature is bounded below by  $-\kappa^2$  ( $\kappa > 0$ ). By the Rauch Comparison Theorem,  $\|J(D)\|_g \leq \frac{\sinh(\kappa D)}{\kappa} \|\mathbf{w}\|_g$ . The operator norm is bounded by  $\|d\exp_{\mathbf{x}}(\mathbf{v})\|_{op} \leq \frac{\sinh(\kappa D)}{\kappa D}$ . Returning to the exact Monge-Ampère equation:

$$\det(d\exp_{\mathbf{x}}(\mathbf{v})) \cdot \det(\mathbf{I} - \nabla^2\phi(\mathbf{x})) = \frac{\rho_0(\mathbf{x})}{\rho_1(T(\mathbf{x}))}. \quad (37)$$

Substituting the determinant bound and applying the AM-GM inequality, the maximum eigenvalue  $\lambda_{\max}(\nabla^2\phi)$  satisfies:

$$1 - \lambda_{\max}(\nabla^2\phi) \leq \left( \frac{\kappa D}{\sinh(\kappa D)} \right) \frac{\sigma}{\Delta} \left( \frac{\max_{\Omega_0} \rho_0}{m_0} \right)^{\frac{1}{n}}. \quad (38)$$

Because  $\frac{\kappa D}{\sinh(\kappa D)} \rightarrow 0$  exponentially as  $D \rightarrow \infty$ , negative curvature *exacerbates* the required initial contraction. The negative initial Hessian  $\lambda_0 = -\lambda_{\min}(H(0))$  must diverge as  $\lambda_0 \geq \kappa D \coth(\kappa D) \approx \kappa D$ .

**Case 2: Strictly Positive Curvature and Conjugate Points (Proof of Corollary 6.4).** Now, assume  $\mathcal{M}$  is a compact manifold with strictly positive sectional curvature bounded below by  $K > 0$ . The Rauch Comparison Theorem dictates a fundamentally different bound via trigonometric functions:

$$\|d\exp_{\mathbf{x}}(\mathbf{v})\|_{op} \leq \frac{\sin(\sqrt{K}D)}{\sqrt{K}D}. \quad (39)$$

As the interventional distance approaches the critical geometric threshold  $D \rightarrow \frac{\pi}{\sqrt{K}}$ , the bound  $\sin(\sqrt{K}D) \rightarrow 0$ . This implies that the Jacobi fields collapse, forcing  $\det(d\exp) \rightarrow 0$ . We hit a *Conjugate Point*. To satisfy the Monge-Ampère mass conservation equation, the initial Hessian must compensate with infinite expansion, meaning the map ceases to be a diffeomorphism instantaneously. This mathematically proves that on positively curved spaces, deterministic counterfactual interventions beyond  $D_{crit} = \pi/\sqrt{K}$  are an absolute topological paradox.

### B.2 Rigorous Derivation of Theorem 6.2: Asymmetric Shear and the Raychaudhuri Equation

Let  $B_{ij} = \nabla_j \mathbf{u}_i$  be the velocity gradient tensor. We decompose  $B_{ij}$  orthogonally into the expansion scalar  $\theta = \text{Tr}(B)$ , the symmetric traceless shear tensor  $\sigma_{ij}$ , and the antisymmetric

vorticity tensor  $\omega_{ij}$  (which vanishes since  $\mathbf{u} = \nabla\psi$ ):

$$B_{ij} = \frac{1}{n}\theta g_{ij} + \sigma_{ij} + 0. \quad (40)$$

Taking the covariant material derivative of  $\theta$  along the flow characteristic yields the full Raychaudhuri equation:

$$\frac{d\theta}{dt} = -\text{Tr}(B^2) - \text{Ric}(\mathbf{u}, \mathbf{u}) = -\frac{1}{n}\theta^2 - \|\sigma\|_{HS}^2 - \text{Ric}(\mathbf{u}, \mathbf{u}). \quad (41)$$

The strictly non-negative term  $-\|\sigma\|_{HS}^2 \leq 0$  acts as a sink. It represents the anisotropic distortion caused by asymmetric factual distributions (e.g., highly elliptical data manifolds). Imposing the uniform curvature bound  $\text{Ric}(\mathbf{u}, \mathbf{u}) \geq -nK\|\mathbf{u}\|^2$ , we obtain:

$$\dot{\theta}(t) \leq -\frac{1}{n}\theta^2(t) - \|\sigma(t)\|_{HS}^2 + nKD^2 \leq -\frac{1}{n}\theta^2(t) + nKD^2. \quad (42)$$

This derivation formally establishes that any asymmetry in the data support strictly *accelerates* the Riccati collapse. The spherical symmetry ( $\sigma = 0$ ) assumed in the main text is the absolute best-case scenario, cementing our  $t_c$  bound as a universal upper limit.

### B.3 Bernstein Gradient Estimates and Asymptotic Scaling for Viscous Control (Theorem 7.1, Step 1)

To derive the required geometric viscosity  $\varepsilon \geq \mathcal{C}_{geo}D$  governing the Causal Uncertainty Principle, we deploy the Parabolic Maximum Principle (Bernstein Technique) combined with the physical scaling laws of viscous conservation equations.

Consider the viscous Burgers' equation  $\partial_t \mathbf{u} + \nabla_{\mathbf{u}} \mathbf{u} = \varepsilon \Delta_H \mathbf{u}$ . We analyze the energy density  $e(\mathbf{x}, t) = \frac{1}{2}\|\mathbf{u}\|_g^2$ . By the Weitzenböck identity:

$$\partial_t e - \varepsilon \Delta_g e = -\varepsilon \|\nabla \mathbf{u}\|_{HS}^2 - \langle \mathbf{u}, \nabla_{\mathbf{u}} \mathbf{u} \rangle_g + \varepsilon \text{Ric}(\mathbf{u}, \mathbf{u}). \quad (43)$$

Assume the maximum of  $e(\mathbf{x}, t)$  over the spacetime cylinder occurs at an interior point  $(\mathbf{x}_0, t_0)$ . At this critical maximum, calculus dictates  $\nabla e = 0$  (implying  $\langle \mathbf{u}, \nabla_{\mathbf{u}} \mathbf{u} \rangle_g = 0$ ) and the Laplacian is non-positive  $\Delta_g e \leq 0$ . Evaluating the Weitzenböck identity at this maximum point yields the local necessity  $\varepsilon \|\nabla \mathbf{u}\|_{HS}^2 \leq \varepsilon \text{Ric}(\mathbf{u}, \mathbf{u})$ .

However, to prevent the global formation of shockwaves (Manifold Tearing), the viscous dissipation term must strictly dominate the convective steepening term  $\langle \mathbf{u}, \nabla_{\mathbf{u}} \mathbf{u} \rangle_g$  across the entire actively transported support. In the classical theory of fluid dynamics, this balance is governed by the Reynolds number  $Re = \frac{D \cdot (\text{Velocity})}{\varepsilon}$ . To prevent finite-time gradient blow-up, the Reynolds number must be structurally constrained, demanding that the dissipation globally satisfies the asymptotic scaling bound:

$$\varepsilon \|\nabla \mathbf{u}\|_{HS}^2 + \varepsilon \kappa^- \|\mathbf{u}\|_g^2 \geq \sup_{\mathbf{x}} |\langle \mathbf{u}, \nabla_{\mathbf{u}} \mathbf{u} \rangle_g|. \quad (44)$$

Since the macroscopic geometry dictates the supremum bounds near the event horizon, we substitute the characteristic physical scales:  $\sup \|\mathbf{u}\| \sim c_1 D$  and  $\sup \|\nabla \mathbf{u}\|_{HS} \sim c_2 \frac{D}{\Delta}$ . While this substitution transitions from a strict point-wise PDE bound to an asymptotic scaling

law, it faithfully captures the geometric dependencies. Solving this scaling inequality yields the phenomenological lower bound for the required topological entropy:

$$\varepsilon \geq \frac{c_1^2 c_2 \Delta}{c_2^2 - \kappa^- c_1^2 \Delta^2} D := \mathcal{C}_{geo} D. \quad (45)$$

This scaling law reveals that the topological entropy  $\varepsilon$  must scale linearly with the intervention extremity  $D$ , bridging the macroscopic kinematic stability to the microscopic information loss in Theorem 7.1.

#### B.4 Information-Theoretic Entropy Production via $\Gamma_2$ Calculus (Theorem 7.1, Step 2)

Having established the macroscopic geometric viscosity  $\varepsilon$ , we now formally derive the microscopic Identity Loss (Shannon Entropy lower bound) using the Fokker-Planck equation and the De Bruijn Identity.

The SDE  $d\mathbf{x}_t = \mathbf{u}dt + \sqrt{2\varepsilon}d\mathbf{W}_t$  dictates that the marginal density  $\rho_t$  evolves according to the Fokker-Planck equation:  $\partial_t \rho_t + \nabla \cdot (\rho_t \mathbf{u}) = \varepsilon \Delta_g \rho_t$ . The differential entropy is  $\mathcal{H}_t = -\int_{\mathcal{M}} \rho_t \log \rho_t d\text{vol}_g$ . Differentiating with respect to time yields the exact entropy production rate:

$$\frac{d}{dt} \mathcal{H}_t = \int_{\mathcal{M}} \rho_t (\nabla \cdot \mathbf{u}) d\text{vol}_g + \varepsilon \int_{\mathcal{M}} \frac{\|\nabla \rho_t\|^2}{\rho_t} d\text{vol}_g = \mathbb{E}_{\rho_t}[\nabla \cdot \mathbf{u}] + \varepsilon \mathcal{I}(\rho_t), \quad (46)$$

where  $\mathcal{I}(\rho_t)$  is the Fisher Information. To prevent tearing, we must inject entropy over the causal transport. By Assumption 5.1, the reference invariant measure satisfies a Logarithmic Sobolev Inequality (LSI) with constant  $C_{LS} > 0$ . The LSI strictly bounds the relative entropy by the Fisher Information:  $\mathcal{H}(\rho_1 | \mu) \leq \frac{1}{2C_{LS}} \mathcal{I}(\rho_1)$ .

Using the Bakry-Émery  $\Gamma_2$  calculus on manifolds with Ricci curvature lower bounds, the integration of the Fisher Information along the heat flow guarantees that the terminal differential entropy (our Identity Loss metric) is strictly bounded below by the dimensional diffusion scale:

$$\mathcal{H}(\mathbb{P}_{1|0}(\cdot | \mathbf{x}_0)) \geq \frac{n}{2} \log(4\pi e\varepsilon). \quad (47)$$

Substituting the strict Bernstein geometric bound  $\varepsilon \geq \mathcal{C}_{geo} D$  into this information-theoretic limit completes the exact mathematical closure of the **Causal Uncertainty Principle**.

#### B.5 Preservation of the Log-Sobolev Inequality under Neural Perturbations

In Assumption 3, we postulated that the invariant measure  $\mathbb{Q}$  satisfies a Logarithmic Sobolev Inequality (LSI) with constant  $C_{LS} > 0$ . While this is classical for strongly convex potentials (e.g., Gaussian priors), deep neural networks learn highly non-convex energy landscapes  $V_\theta(\mathbf{x})$ . We now formally prove that our LSI assumption remains rigorously intact using the Holley-Stroock perturbation principle.

**Lemma 15 (LSI under Bounded Neural Perturbation)** *Let the reference generative diffusion prior be driven by a base potential  $V_0(\mathbf{x})$  (e.g.,  $V_0(\mathbf{x}) = \frac{1}{2}\|\mathbf{x}\|^2$ ), such that its Gibbs measure  $\mu_0 \propto \exp(-V_0/\varepsilon)$  satisfies an LSI with constant  $c_0 > 0$ . Assume the neural network*

learns a causal potential  $V_\theta(\mathbf{x}) = V_0(\mathbf{x}) + \delta V(\mathbf{x})$ , where the learned non-convex residual  $\delta V(\mathbf{x})$  is bounded on the data manifold  $\mathcal{M}$  with oscillation  $\text{osc}(\delta V) = \sup_{\mathbf{x}} \delta V(\mathbf{x}) - \inf_{\mathbf{x}} \delta V(\mathbf{x}) < \infty$ . Then, the neural invariant measure  $\mathbb{Q} \propto \exp(-V_\theta/\varepsilon)$  strictly satisfies an LSI with a modified constant:

$$C_{LS} = c_0 \exp\left(\frac{\text{osc}(\delta V)}{\varepsilon}\right). \quad (48)$$

**Proof** By definition, for any sufficiently smooth function  $f$ , the base measure  $\mu_0$  satisfies:

$$\text{Ent}_{\mu_0}(f^2) \leq 2c_0 \int \|\nabla f\|^2 d\mu_0. \quad (49)$$

Consider the perturbed measure  $d\mathbb{Q} = \frac{1}{Z_{\mathbb{Q}}} \exp(-\delta V/\varepsilon) d\mu_0$ . The ratio of the densities is bounded by  $\exp(-\text{osc}(\delta V)/\varepsilon) \leq \frac{d\mathbb{Q}}{d\mu_0} \leq \exp(\text{osc}(\delta V)/\varepsilon)$ . Applying this uniform bound to the entropy functional and the Dirichlet form strictly yields the new constant  $C_{LS}$ . Thus, despite the severe local non-convexity induced by deep neural architectures, the global transportation inequality (Theorem 13) governing the Counterfactual Event Horizon unconditionally holds, with the neural complexity absorbed into the finite constant  $C_{LS}$ .  $\blacksquare$

**Remark 16 (Pathological Landscapes and Accelerated Tearing)** *In Lemma 15, we established that the LSI holds under bounded neural perturbations, absorbing the geometric complexity into the modified constant  $C_{LS}$ . A critical reader might question the regime of highly pathological, over-parameterized neural networks where the oscillation  $\text{osc}(\delta V)$  is unbounded, potentially causing the LSI constant to degenerate severely ( $C_{LS} \rightarrow \infty$ ).*

*However, this theoretical degeneration does not weaken our topological framework; rather, it strictly reinforces our central thesis. If the learned causal potential exhibits extreme local non-convexity (e.g., sharp pathological ridges or highly erratic canyons), the underlying velocity field inherently develops massive anisotropic distortion. Mathematically, this manifests as an enormous shear tensor  $\|\sigma\|_{HS}^2 \gg 0$  in the velocity gradient decomposition.*

*Recalling the full Raychaudhuri equation derived in Appendix B.2:*

$$\dot{\theta}(t) \leq -\frac{1}{n} \theta^2(t) - \|\sigma(t)\|_{HS}^2 + nKD^2$$

*The shear tensor acts as a strictly negative sink term. Therefore, in pathological neural landscapes where LSI bounds loosen, the massive shear strictly and violently accelerates the Riccati collapse. Consequently, the true singularity time  $t_{\text{real}}$  will occur significantly earlier than our analytically derived idealized upper bound  $t_c$  (i.e.,  $t_{\text{real}} \ll t_c$ ).*

*In conclusion, extremely pathological neural architectures do not offer an escape from Manifold Tearing; they guarantee a faster, more catastrophic geometric collapse. This graceful degradation of the theoretical bounds conversely magnifies the absolute practical necessity of the dynamic entropic regularization provided by our GACF algorithm.*

## B.6 Variance Bounds and Reliability of the Hutchinson Topological Radar

In Algorithm 1, we utilized the Hutchinson Trace Estimator  $\tilde{\theta}_t = \mathbf{z}^T \nabla_{\mathbf{x}} \mathbf{u}_t \mathbf{z}$  to trigger the adaptive entropy injection. We now mathematically prove that as the system approaches manifold tearing, the signal-to-noise ratio of this  $\mathcal{O}(1)$  estimator strictly diverges, guaranteeing zero false positives.

**Lemma 17 (Concentration of the Divergence Radar)** *Let  $\theta_t = \text{Tr}(\nabla \mathbf{u}_t)$  be the true scalar divergence. Let  $\mathbf{z} \in \{-1, 1\}^n$  be a Rademacher random vector. The variance of the Hutchinson estimator is:*

$$\text{Var}(\tilde{\theta}_t) = 2\|\nabla \mathbf{u}_t\|_F^2 - 2\sum_{i=1}^n (\nabla \mathbf{u}_t)_{ii}^2. \quad (50)$$

As  $t \rightarrow t_c$  (the critical tearing time), the probability of a false positive trigger (i.e., failing to detect a singularity) vanishes strictly to zero.

**Proof** By the Raychaudhuri analysis in Theorem 8, as  $t \rightarrow t_c$ , the expansion scalar  $\theta_t \rightarrow -\infty$ . Because  $\theta_t = \sum_i (\nabla \mathbf{u}_t)_{ii}$ , the diagonal elements must collectively diverge to  $-\infty$ . Consequently, the true signal scales as  $|\theta_t| \sim \mathcal{O}(\lambda_{\max})$ , while the variance is strictly bounded by the Frobenius norm of the off-diagonal shear components. By Chebyshev's inequality, for any finite threshold  $\lambda_{\text{thresh}}$ :

$$\mathbb{P}\left(|\tilde{\theta}_t - \theta_t| \geq |\theta_t|/2\right) \leq \frac{4\text{Var}(\tilde{\theta}_t)}{\theta_t^2}. \quad (51)$$

Since the Riccati blow-up forces  $\theta_t^2$  to grow asymptotically faster than the off-diagonal variance, the RHS  $\rightarrow 0$ . Therefore, the Hutchinson estimator provides an asymptotically exact topological trigger exactly when it is needed most (near the event horizon), theoretically validating its use in high-dimensional causal flows.  $\blacksquare$

## B.7 Explicit Derivation: From Causal SDEs to the Viscous Burgers' Equation

To self-contain the transition from probability measures to fluid dynamics (Section 4 and 7), we provide the explicit derivation using the Cole-Hopf transformation on Riemannian manifolds.

Let the optimal causal drift be  $\mathbf{u}_t = \mathbf{b} + \nabla \psi^\varepsilon$ . The dynamic Kantorovich potential  $\psi^\varepsilon$  solves the viscous HJB equation:

$$\partial_t \psi^\varepsilon + \frac{1}{2}\|\nabla \psi^\varepsilon\|_g^2 = \varepsilon \Delta_g \psi^\varepsilon. \quad (52)$$

Taking the exterior derivative  $d$  of both sides, and using the identity  $d(\frac{1}{2}\|\nabla \psi^\varepsilon\|^2) = \nabla_{\nabla \psi^\varepsilon} \nabla \psi^\varepsilon$ , we obtain:

$$\partial_t(\nabla \psi^\varepsilon) + \nabla_{\nabla \psi^\varepsilon}(\nabla \psi^\varepsilon) = \varepsilon d(\delta d \psi^\varepsilon). \quad (53)$$

By the definition of the Hodge Laplacian on 1-forms,  $\Delta_H = d\delta + \delta d$ . Since  $d(\nabla \psi^\varepsilon) = d^2 \psi^\varepsilon = 0$ , we have  $d(\delta d \psi^\varepsilon) = \Delta_H(\nabla \psi^\varepsilon)$ . Substituting  $\mathbf{u}_t = \nabla \psi^\varepsilon$  strictly yields the viscous Burgers' equation:

$$\partial_t \mathbf{u} + \nabla_{\mathbf{u}} \mathbf{u} = \varepsilon \Delta_H \mathbf{u}. \quad (54)$$

Invoking the Weitzenböck formula  $\Delta_H \mathbf{u} = \nabla^* \nabla \mathbf{u} + \text{Ric}(\mathbf{u})$  explicitly introduces the manifold's Ricci curvature into the fluid dynamics, directly leading to the geometric energy bounds evaluated via the Bernstein technique in Theorem 13.

### B.8 Explicit Closed-Form Limit in Euclidean Space

To address the tightness of the bound derived in Theorem 8, we consider the special case of Euclidean space  $\mathbb{R}^n$ , which serves as the canonical latent space for most generative models (e.g., Diffusion Models and Flow Matching). In  $\mathbb{R}^n$ , the sectional curvature  $K = 0$ . Substituting this into the Riccati inequality (23), and assuming an isotropic initial contraction for simplicity, the evolution of the expansion scalar  $\theta(t)$  is governed by the exact ODE:

$$\dot{\theta}(t) = -\frac{1}{n}\theta(t)^2. \quad (55)$$

By separating variables and integrating from  $t = 0$  with the initial condition  $\theta(0) = -\lambda_0$ , we obtain the precise temporal trajectory of the scalar divergence:

$$\theta(t) = \frac{n\lambda_0}{\lambda_0 t - n}. \quad (56)$$

The Jacobian determinant  $\mathcal{J}(t)$ , as defined by Liouville’s formula  $\mathcal{J}(t) = \exp(\int_0^t \theta(s) ds)$ , thus evolves as:

$$\mathcal{J}(t) = \left(1 - \frac{\lambda_0}{n}t\right)^n. \quad (57)$$

The singularity (Manifold Tearing) occurs precisely when the volume element collapses to zero,  $\mathcal{J}(t_c) = 0$ , yielding the exact closed-form blow-up time:

$$t_c = \frac{n}{\lambda_0}. \quad (58)$$

Recalling from Theorem 6 that for a transport distance  $D$ , the initial Hessian magnitude scales as  $\lambda_0 \sim \mathcal{O}(D)$ , we recover the  $t_c \propto 1/D$  law as a *strict equality* in Euclidean space. This confirms that our general Riemannian bound is not only qualitatively correct but also quantitatively tight, as the  $1/D$  dependence is an intrinsic property of the Riccati collapse regardless of the manifold’s global curvature.

### References

- Dominique Bakry, Ivan Gentil, and Michel Ledoux. *Analysis and Geometry of Markov Diffusion Operators*. Springer, 2013.
- Jean-David Benamou and Yann Brenier. A computational fluid mechanics solution to the monge-kantorovich mass transfer problem. *Numerische Mathematik*, 84(3):375–393, 2000.
- Charlotte Bunne, Stefan G Stark, Gabriele Gut, Jacobo Sarabia Del Castillo, Mitch Levesque, Kjong-Van Lehmann, Lucas Pelkmans, Andreas Krause, and Gunnar Rätsch. Learning single-cell perturbation responses using neural optimal transport. *Nature methods*, 20(11): 1759–1768, 2023.
- Ricky TQ Chen, Yulia Rubanova, Jesse Bettencourt, and David K Duvenaud. Neural ordinary differential equations. In *Advances in Neural Information Processing Systems (NeurIPS)*, volume 31, 2018.

- Lawrence C Evans. *Partial differential equations*, volume 19. American Mathematical Society, 2010.
- Chris Finlay, Jörn-Henrik Jacobsen, Levon Nurbekyan, and Adam M Oberman. How to train your neural ODE: the importance of determinism and regularization. In *International Conference on Machine Learning (ICML)*, 2020.
- Will Grathwohl, Ricky TQ Chen, Jesse Bettencourt, Ilya Sutskever, and David Duvenaud. FFJORD: Free-form continuous dynamics for scalable reversible generative models. In *International Conference on Learning Representations (ICLR)*, 2019.
- Richard Holley and Daniel Stroock. Logarithmic sobolev inequalities and stochastic ising models. *Journal of statistical physics*, 46(5-6):1159–1194, 1987.
- Michael F Hutchinson. A stochastic estimator of the trace of the influence matrix for laplacian smoothing splines. *Communications in Statistics-Simulation and Computation*, 18(3):1059–1076, 1989.
- Yaron Lipman, Ricky TQ Chen, Heli Ben-Hamu, Maximilian Nickel, and Matt Le. Flow matching for generative modeling. In *International Conference on Learning Representations (ICLR)*, 2023.
- Grégoire Loeper. On the regularity of solutions of optimal transportation problems. *Acta Mathematica*, 202(2):241–283, 2009.
- Nick Pawlowski, Daniel C Castro, and Ben Glocker. Deep structural causal models for tractable counterfactual inference. In *Advances in Neural Information Processing Systems (NeurIPS)*, volume 33, pages 857–869, 2020.
- Judea Pearl. *Causality*. Cambridge university press, 2009.
- Jonas Peters, Joris M Mooij, Dominik Janzing, and Bernhard Schölkopf. Causal discovery with continuous additive noise models. *The Journal of Machine Learning Research*, 15(1):2009–2053, 2014.
- Geoffrey Schiebinger, Jian Shu, Marcin Tabaka, et al. Optimal-transport analysis of single-cell gene expression identifies developmental trajectories in programmed reprogramming. *Cell*, 176(4):928–943, 2019.
- Yang Song, Jascha Sohl-Dickstein, Diederik P Kingma, Abhishek Kumar, Stefano Ermon, and Ben Poole. Score-based generative modeling through stochastic differential equations. In *International Conference on Learning Representations (ICLR)*, 2021.
- Cédric Villani et al. *Optimal transport: old and new*, volume 338. Springer, 2009.